Palaeogeography, Palaeoclimatology, Palaeoecology 656 (2024) 112595

Contents lists available at ScienceDirect

Palaeogeography, Palaeoclimatology, Palaeoecology

journal homepage: www.elsevier.com/locate/palaeo

Reconstruction of hydroclimate variability in southern Laos from 1885 to 2019 based on *Pinus latteri* tree-ring data

Nakhonekham Xaybouangeun [a,b,c], Zaw Zaw [a,d,*], Rao-Qiong Yang [a], Shankar Panthi [a], Dao-Xiong Gao [a], Viengsy Paothor [e], Ze-Xin Fan [a,d,*]

[a] *CAS Key Laboratory of Tropical Forest Ecology, Xishuangbanna Tropical Botanical Garden, Chinese Academy of Sciences, Menglun, Mengla, Yunnan 666303, China*
[b] *College of Life Sciences, University of Chinese Academy of Sciences, Beijing 100049, China*
[c] *Science and Innovation Research Institute, Ministry of Education and Sports, Vientiane 067, Laos*
[d] *Ailaoshan Station of Subtropical Forest Ecosystem Studies, Xishuangbanna Tropical Botanical Garden, Chinese Academy of Sciences, Jingdong, Yunnan 676209, China*
[e] *Faculty of Forest Science, The National University of Laos, Vientiane 7322, Laos*

ARTICLE INFO

Editor: Howard Falcon-Lang

Keywords:
Dendroclimatology
Pinus latteri
El Niño-Southern Oscillation (ENSO)
Southern Laos
Standardized Precipitation-Evapotranspiration Index (SPEI)
Tree rings

ABSTRACT

The climate of Southeast Asia is influenced by the Asian monsoon systems, and inter-annual hydroclimate variability exerts a significant impact on forest ecosystems and agricultural productivity in this region. To improve our understanding of long-term drought variability, this study established ring-width chronologies for *Pinus latteri* trees at three sites in southern Laos. Site chronologies show negative correlations with temperature and positive correlations with precipitation, the self-calibrated Palmer Drought Severity Index (scPDSI), and the Standardized Precipitation-Evapotranspiration Index (SPEI) during the dry and wet months. The regional composite chronology shows the strongest correlation ($r = 0.657$, $p < 0.001$) with SPEI during March–August, indicating that the radial growth of *P. latteri* in southern Laos is primarily influenced by moisture conditions during the dry-to-wet season. A well-calibrated regression model was employed to reconstruct the variability of March–August SPEI for the period 1885–2019, explaining 43.1 % of the observed SPEI variance during the calibration period 1960–2019. The reconstruction records inter-annual to decadal-scale drought variability in southern Laos including eleven extreme dry years and seven extreme wet years. Notably, the frequency of extreme dry and wet events has increased since the 1970s. The reconstruction shows spectral peaks with periodicities of 2.3–3.1 years and displays negative correlations with sea surface temperatures (SSTs) in the tropical Pacific and Indian oceans, indicating that hydroclimatic variations in southern Laos are driven by large-scale ocean-atmospheric circulations.

1. Introduction

Global climate change, primarily characterized by global warming and largely attributed to anthropogenic activities, has led to shifts in precipitation patterns due to alternations in ocean-atmospheric circulations (AghaKouchak et al., 2014; IPCC, 2023). The rise in global temperatures has substantially increased the frequency and intensity of drought events in recent years (Trenberth et al., 2004; IPCC, 2023). Prolonged droughts have far-reaching societal and ecological impacts, severely affecting human societies, agriculture, and vegetation (Vicente-Serrano et al., 2010; Eslamian et al., 2017). Forest ecosystems are facing the threats of climate change, primarily due to droughts induced by global change (Hartmann et al., 2022), which contribute to the increasing frequency and intensity of fires, tree mortality, and declining productivity in forests (Stephens et al., 2013; Doughty et al., 2015; Mukherjee et al., 2018). Southeast Asia harbors approximately 15 % of the world's tropical forests (Stibig et al., 2014; FAO, 2020), serving as vital tropical biodiversity hotspots and playing a crucial role in maintaining global carbon balance and biodiversity conservation (Estoque et al., 2019). Despite their significance, these forests face threats from human activities, including land-use changes and the impacts of global climatic change (Wilcove et al., 2013; Estoque et al., 2019).

In recent decades, many regions worldwide have experienced drought conditions, exacerbated by climate change (Dai, 2010; Kang

* Corresponding authors at: CAS Key Laboratory of Tropical Forest Ecology, Xishuangbanna Tropical Botanical Garden, Chinese Academy of Sciences, Menglun, Mengla, Yunnan 666303, China.

E-mail addresses: zawzaw@xtbg.ac.cn (Z. Zaw), fanzexin@xtbg.org.cn (Z.-X. Fan).

https://doi.org/10.1016/j.palaeo.2024.112595
Received 1 August 2024; Received in revised form 4 November 2024; Accepted 4 November 2024
Available online 8 November 2024

and Sridhar, 2020). The Lower Mekong Basin, including Laos, has endured several severe droughts over the past three decades, which have caused significant crop losses, reduced yields in fisheries and livestock, increased salinity intrusion, and domestic and industrial water shortages (Guo et al., 2017; Ruiz-Barradas and Nigam, 2018; Mekong River Commission, 2019). Notable events include the prolonged drought of 1991–1994 and the extremely dry conditions of 2015–2016, with the latter resulting in an estimated $1.7 billion in economic losses in Thailand and affecting over 9.56 million people (Mekong River Commission, 2019; Kang et al., 2021). Historical drought reconstructions in Myanmar indicate that six of twelve major famines, resulting in millions of deaths, coincided with periods of drought in southern regions (Zaw et al., 2020). Additionally, a drought reconstruction from northern Vietnam identified a prolonged, nearly 30-year drought in the mid-18th century, which coincided with concurrent conditions in northwestern Thailand, suggesting the occurrence of 18th-century "mega-drought" across Indochina (Sano et al., 2009).

The climate of Southeast Asia is strongly influenced by inter-annual to decadal hydroclimate variability driven by El Niño-Southern Oscillation (ENSO), as the region is impacted by ocean-atmospheric circulations across the tropical Pacific and Indian oceans (Pumijumnong et al., 2023). However, climate stations in this region are sparsely distributed, and the existing records generally cover short time spans, hindering the analysis of long-term patterns in regional hydroclimate variability (Zaw et al., 2020, 2021; Pumijumnong et al., 2023). To better understand regional hydroclimate variations and their impacts on tropical forests, it is essential to establish high-resolution climate proxies, including tree rings, in Southeast Asia.

Tree rings have been extensively used as proxies to study the long-term perspective of hydroclimate variability in Southeast Asia (Panthi et al., 2017; Pumijumnong et al., 2023), with research focusing on teak (e.g., Pumijumnong, 2013; Zaw et al., 2020, 2021) and pine (e.g., Pumijumnong et al., 2021, 2023; Yang et al., 2022) species. These studies covered a wider spatial scale and environmental gradient, encompassing regions such as Cambodia (e.g., Zhu et al., 2012), Thailand (e.g., Pumijumnong and Eckstein, 2010; Vlam et al., 2014; Lumyai et al., 2020; Pumijumnong et al., 2023), Myanmar (e.g., Zaw et al., 2020, 2021), Vietnam (e.g., Buckley et al., 2010, 2017), and southern China (e.g., Sharma et al., 2022; Yang et al., 2022; Xu et al., 2024). These dendroclimatic studies have revealed a strong sensitivity to climate variations, making them valuable for hydroclimate reconstructions across the Southeast Asian region (e.g., Buckley et al., 2017; Pumijumnong et al., 2023). In northern Laos, a tree-ring oxygen isotope ($\delta^{18}O$) chronology from *Fokienia hodginsii* trees on Phu Leuy Mountain shows a significant negative correlation with the regional Palmer drought severity index (PDSI) from May to October (Xu et al., 2011). However, there remains a lack of dendroclimatic studies focusing on past hydroclimate reconstructions in Laos (Buckley et al., 2007; Xu et al., 2011).

Pinus latteri is widely distributed across tropical Southeast Asia (Averyanov et al., 2014). Growth of *P. latteri* is highly sensitive to year-to-year hydroclimate variabilities, and tree-ring data of this species serve as climate proxies and provide the opportunity for paleoclimate reconstruction across the tropical regions of Southeast Asia (Pumijumnong et al., 2023). This study aims to develop ring-width chronologies of *P. latteri* trees and reconstruct regional drought variability in southern Laos. We aimed to answer three questions: 1) What climatic factors limit the radial growth of *P. latteri* trees in southern Laos? 2) How does regional hydroclimate variability, including dry-wet events and drought severity, shift under regional warming? 3) What is the relationship between hydroclimate variability in southern Laos and sea surface temperatures (SSTs) anomalies in the tropical Pacific Ocean and Indian Ocean? We hypothesized that 1) the radial growth of *P. latteri* trees in southern Laos is significantly influenced by moisture conditions during the dry and wet seasons, and 2) drought extremes in southern Laos have intensified due to weakened monsoon patterns, with ENSO activities playing a crucial role in driving regional drought variability.

2. Materials and methods

2.1. Study area and climatic conditions

The study area is situated in southern Laos, encompassing three provinces: Savannakhet (Dong Phou Vieng National Protected Area, DPV), Salavan (Xe Sap National Protected Area, TX), and Champasack (Natural Seed Source NongNa Conservation Area for *P. laterri*, Mounlapamok, MM). Southern Laos is characterized by diverse topography, including the Annamite Mountain Ranges bordering Vietnam to the East, which features rugged terrain with peaks reaching considerable elevations (Lao PDR, 2021). Additionally, the Mekong River to the West has significantly influenced the region's diverse topography, contributing extensive river valleys and floodplains. The study region hosts diverse tropical forests, including evergreen, mixed evergreen, semi-evergreen, and dry deciduous forests, as well as tropical savannas.

The climate of Laos is predominantly shaped by seasonal monsoon winds that influence weather patterns across Southeast Asia. This monsoon cycle arises from the seasonal temperature contrast between the expansive Asian landmass and the surrounding oceans (Wang et al., 2000). During winter, the continental air cools, becomes dense, and flows southward, creating the northeast monsoon. This dry, cool airflow, originating over land, dominates Laos from November to April, leading to a distinct dry season. In summer, the pattern reverses as warmer continental air rises, creating a low-pressure zone that draws in moisture-laden air masses from the oceans. These air masses accumulate moisture as they move across the ocean, releasing it as precipitation upon reaching the continent. This southwesterly airflow, or southwest monsoon, brings substantial rainfall to Laos from May to October, marking the wet season. Consequently, the monsoon cycle produces two main seasons in Laos: a wet season, influenced by the southwest monsoon, and a dry season, dominated by the northeast monsoon (https://bluegreenatlas.com/climate/laos_climate.html; FAO, MONREC and MAF, 2022).

Southern Laos has a typical tropical monsoon climate, characterized by a distinct dry season from November to April and a wet season from May to October due to precipitation seasonality. Temperatures range from 25 °C to 27 °C in the plains, varying slightly with elevation and seasons (Lao PDR, 2021). Summer monsoon precipitation is influenced by the monsoonal winds from the Indian Ocean, with the heaviest rainfall occurring from July to October, contributing approximately 70 % of the total annual precipitation (Lao PDR, 2013, 2021). The northeast monsoon, which follows the withdrawal of the summer monsoon, brings dry continental air masses, creating drier climate conditions. According to the regional climate series derived from the gridded Climatic Research Unit (CRU) data, the annual mean temperature and total precipitation for southern Laos from 1960 to 2019 were 25.8 °C and 2022 mm, respectively (Fig. 2). Meanwhile, meteorological stations in Savannakhet, Salavan, and Pakse reported annual mean temperatures of 26.4 °C, 27.1 °C, and 27.6 °C, with total annual precipitation of 1489 mm, 2138 mm, and 2069 mm, respectively.

2.2. Tree-core collection and chronology building

Pinus latteri, commonly known as Tenasserim pine or two-needle pine, is widely distributed across the tropics of Southeast Asia, including Cambodia, Laos, Malaysia, Myanmar, the Philippines, Vietnam, Thailand, and parts of southern China. This species grows at elevations ranging from sea level up to 1200 m and can reach heights of up to 45 m, with a diameter at breast height (DBH) of up to 1.5 m. The leaves consist of two needles per fascicle, measuring 20–30 cm in length. Typically, *P. latteri* grows in pure stands or is mixed with dipterocarp species in lowland, periodically inundated areas with infertile soils that support a high diversity of native shrubby, herbaceous, and epiphytic

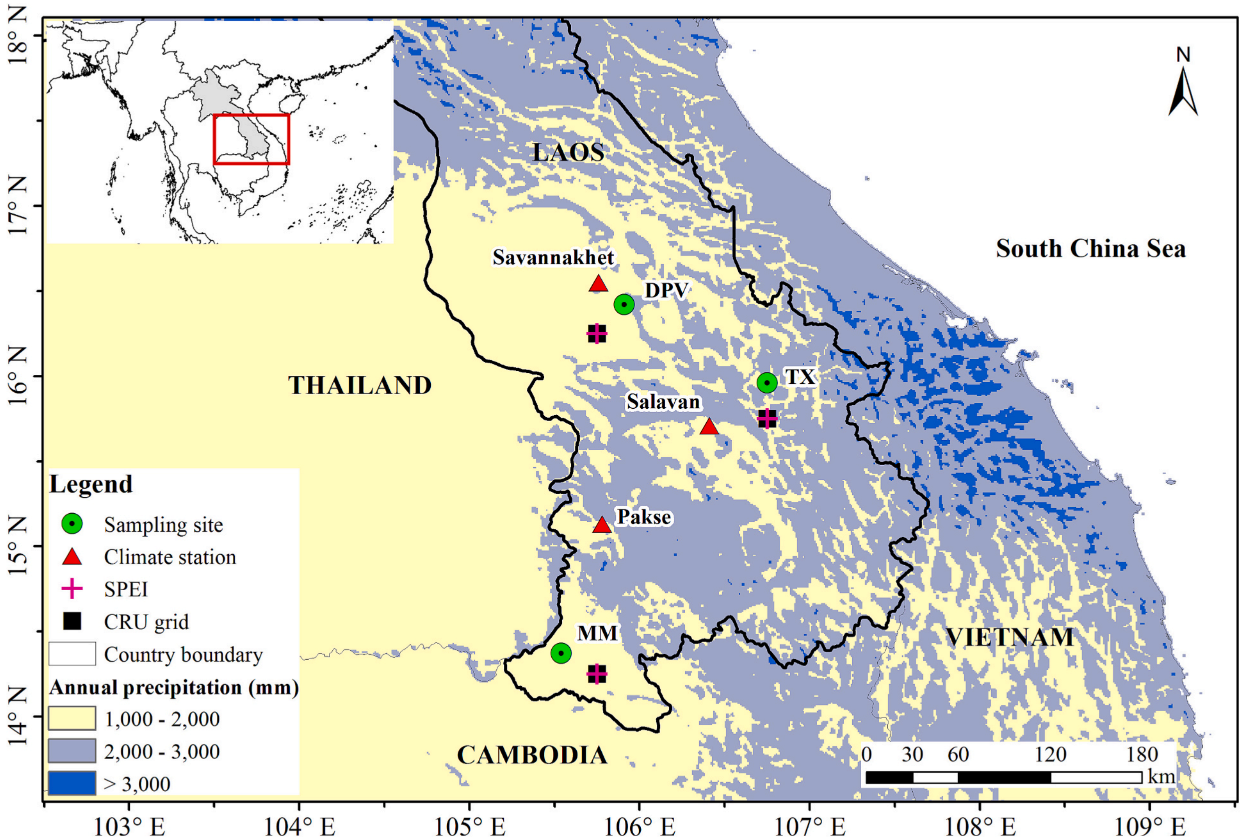

Fig. 1. Locations of *Pinus latteri* tree-ring sampling sites (green circles), meteorological stations (red triangles), and CRU grid points (black squares) in southern Laos. DPV, Dong Phou Vieng; TX, Xe Sap; MM, Mounlapamok. The spatial data of total annual precipitation from 1979 to 2013 was accessed from "Climatologies at High Resolution for the Earth's Land Surface Areas" (https://chelsa-climate.org) at a 30 arcsec (~1 km) horizontal resolution. (For interpretation of the references to colour in this figure legend, the reader is referred to the web version of this article.)

Table 1
Details on sampling sites and statistics of *Pinus latteri* residual chronologies in southern Laos.

Statistics	DPV	TX	MM	SLC
Latitude (°N)	16.42	15.96	14.37	–
Longitude (°E)	105.91	106.75	105.54	–
Elevation (m a.s.l.)	200	990	125	–
No. of trees	24	27	28	79
No. of cores	39	40	44	123
First year	1810	1810	1890	1810
Last year	2019	2019	2019	2019
Mean segment length (MSL, year)	171	121	101	130
Average growth rate (mm/year)	1.155	1.717	2.161	1.698
Median growth rate (mm/year)	1.011	1.570	1.969	1.536
Standard deviation (mm/year)	0.603	0.849	0.987	0.821
Gini coefficient (Gini)	0.283	0.279	0.251	0.270
Mean inter-series correlation (Rbar)	0.318	0.183	0.284	0.161
Expressed population signal (EPS)	0.948	0.900	0.946	0.959
Signal-to-noise ratio (SNR)	18.177	8.989	17.434	23.582

DPV, Dong Phou Vieng; TX, Xe Sap; MM Mounlapamok; SLC, regional Southern Laos composite chronology. Gini, Rbar, EPS, and SNR were calculated after detrending.

plants (Averyanov et al., 2014; Thomas, 2019). *P. latteri* can tolerate high temperatures and drought, thriving in poor soils, which makes it a common species for afforestation efforts. As an essential commercial tree species, its wood and resin are valuable raw materials for paper and ink production. In Laos, this pine species is commonly found in the provinces of Houaphanh, Xiangkhuang, Vientiane, Bolikhamxai, Khammouan, Savannakhet, Salavan, Champasack, Sekong, and Attapeu. Pumijumnong et al. (2021) studied the cambial dynamics of *P. latteri* in subtropical Thailand over two consecutive growing seasons and found increased cambial growth activity from May to September.

Tree-core samples of *P. latteri* were taken from natural pine forests at three sites in southern Laos (Fig. 1), using a borer with a 5.15 mm inner diameter. The elevation of the sampling sites ranges from 125 m to 990 m a.s.l., with a mean elevation of 438 m a.s.l. (Table 1). Increment cores were sampled from mature and healthy trees, and a total of 226 cores from 152 trees were sampled from the three sites in July 2020. Two cores were taken from each tree, about 1.3 m above the ground, in perpendicular directions from either upslope or lateral positions on the main stem. Samples were properly labeled and air-dried in the laboratory. The surface of each core was smoothed using sandpapers of successively finer grit sizes, ranging from 200 to 2000 grits. Ultimately, the xylem structures (tracheids and rays) and annual ring boundaries were clearly visible under a stereomicroscope (×40 magnification). Tree-ring widths from each core were measured with a precision of 0.001 mm using the LINTAB™6 measuring system. Tree-ring measurements were crossdated to their calendar year of formation using TSAP-Win software (Rinn, 2003), and the crossdating was further checked with the COFECHA software (Holmes, 1983). In total, 123 cores (79 trees) from the three sites were well crossdated and used for further analyses (Table 1), while 73 trees (103 cores) were not crossdated due to their individual growth patterns.

The raw series were detrended by applying a fixed 30-year cubic spline curve with a 50 % frequency-response cut-off (Cook and Peters, 1997), using the "dplR" package (Bunn, 2008) in R programme (R Core Team, 2024). Standardization preserves growth variabilities related to climate signals while removing signals related to biological growth trends and minimizing stand dynamics-related noise in the tree-ring time series. The detrended series were then averaged into a mean chronology for each site by calculating the bi-weight robust mean to minimize the impact of outliers (Cook and Kairiukstis, 1990). We also calculated the mean inter-series correlation (Rbar) and the expressed population signal (EPS) to evaluate the reliability of site chronologies. EPS assesses whether the chronology represents the entire population, while Rbar indicates growth synchrony among trees. Both Rbar and EPS were computed over a 30-year window with a 15-year overlap. Chronology estimates were deemed reliable when EPS surpassed an arbitrary threshold of 0.85 (Wigley et al., 1984). The detrending software generated two types of tree-ring chronologies (i.e., standard and residual) for each study site. However, we observed significant autocorrelation in the standard chronologies, which can influence data interpretation and reduce the precision of dendrochronological reconstructions. To address this, we selected residual chronologies for further analyses, as they are free of autocorrelation through autoregressive modeling and retain the most conservative indicators of growth drivers (Cook and Kairiukstis, 1990).

The three site chronologies (Fig. S3) are positively correlated with each other (Table S2) for the common period 1890–2019, with the first principal component (PC#1) explaining 61.44 % of the total variance (Table S3). Furthermore, all three site chronologies showed similar growth-climate relationships (Fig. S4). We, therefore, combined all the raw ring-width series from the three study sites to develop a regional southern Laos composite chronology, hereafter referred to as the Southern Laos Chronology (SLC) (Fig. 3). We followed the same procedure to standardize the regional composite chronology as three site chronologies.

2.3. Climate data

The local climate stations are located far from the tree-ring sampling sites (Table S1), and the available climate data are short-spanned (49 years; 1971–2019) for computing the climate sensitivity analysis. Hence, we extracted climatic data from the CRU with a spatial resolution of 0.5 degrees (Barichivich et al., 2023; CRU TS4.07) via the KNMI Climate Explorer (Trouet and Van Oldenborgh, 2013). The climate data included maximum (Tmx), mean (Tmp), and minimum (Tmn) temperatures, as well as precipitation (Prec) and self-calibrated Palmer Drought Severity Index (scPDSI). Meanwhile, we extracted gridded Standardized Precipitation-Evapotranspiration Index (SPEI) datasets from the Global SPEI database at half-degree spatial resolution (Beguería et al., 2023; SPEIbase v.2.9; https://spei.csic.es/). SPEI, a meteorological drought index, measures the standardized difference between water supply and demand and quantifies drought using the FAO-56 Penman-Monteith method for estimating potential evapotranspiration (Vicente-Serrano et al., 2010). We calculated regional climatic conditions for southern Laos by averaging the data from three CRU grid points for the period 1960–2019. The gridded regional climate data showed strong positive correlations with the averaged climate data of the three meteorological stations (Fig. S2).

2.4. Growth-climate relationships

We computed bootstrapped correlation analyses between residual chronologies of *P. latteri* and monthly CRU climatic variables to evaluate the growth-climate relationships across the three sites, as well as for the regional SLC chronology. Correlation coefficients were computed over a 15-month period spanning from the previous August to the current October for the period 1960–2019. We also computed correlations by averaging climates of different months to evaluate the most dominant seasonal climate variable that limits the growth of *P. latteri* trees in southern Laos. We further conducted a moving correlation analysis to evaluate the temporal stability of tree growth-climate relationships from 1960 to 2019, using a 30-year window with a 2-year offset, by using the R package "treeclim" (Bunn, 2008).

2.5. SPEI reconstruction

Correlation analysis was performed at different dendroclimatic windows: monthly (previous August to current October), seasonal (dry season—November to April; wet season—May to October), yearly (January to December), and dry-to-wet months (March to July; March to August). We reconstructed the SPEI at a regional scale in southern Laos based on the highest correlations with dry-to-wet month climate. We developed a calibration model by computing simple linear regression between the SLC chronology and regional SPEI for the period 1960–2019. We further analyzed several statistical tests, including correlation coefficient (r), variance explained (r^2), standard error (SE), F-test, and Durbin–Watson statistics (DW) for residual autocorrelation, to assess the robustness of the calibration model. After evaluating the calibration model, we applied a 'transfer function' (Fritts, 1976) to predict past SPEI variability in southern Laos, using the SLC chronology as the predictor and observed SPEI as the predictand. We then used the leave-one-out cross-validation method (LOOCV, Michaelsen, 1987) and the spilt-sample validation method (Meko and Graybill, 1995) to verify our reconstruction. The LOOCV method verified the reliability of the predicted (reconstructed) SPEI using several tests, including product mean test (Pmt), sign-test (ST), root mean square error (RMSE), and reduction of error (RE) (Michaelsen, 1987). Meanwhile, the split-sample method divided the calibration period into two equal subperiods for calibration (1960–1989) and verification (1990–2019) and validated the predictive skills of the reconstruction by evaluating the correlation coefficient (r), coefficient of efficiency (CE), and reduction of error (RE). We cut off the reconstruction at the point where the EPS value dropped below 0.85 (Fritts, 1976). We evaluated the anomalies in the reconstructed SPEI as extremely dry/wet years and dry/wet years. The extremely dry and wet years were identified when the reconstructed SPEI values were 1.5 standard deviations (SD) lower (i.e., mean–1.5SD) and higher (mean + 1.5SD) than the mean value, respectively. Meanwhile, years with SPEI values falling below the mean–1SD were categorized as dry, while those falling above the mean + 1SD were classified as wet. To determine the frequency and intensity of extreme events, we calculated the number of such events occurring within 30-year intervals over time. Dry/wet periods were identified when the SPEI reconstruction, filtered with a 10-year smoothing spline, was below or above the mean value (0.095).

2.6. Spatial representativeness and teleconnections

We examined the spatial representativeness of the reconstructed SPEI series by computing correlations with regional gridded land surface climate variables (Tmx and Prec) in the field over the Southeast Asia region. We further assessed the association of our reconstructed SPEI with spatial SSTs variations in the field. Spatial correlation analysis for the period 1960–2019 was conducted using the KNMI Climate Explorer (Trouet and Van Oldenborgh, 2013; http://climexp.knmi.nl). We tested the periodicities in our reconstructed SPEI series using both the Morlet global wavelet spectrum (Grinsted et al., 2004) and Multi-Taper spectral analysis (Mann and Lees, 1996).

We also compared the dry-wet periods in our SPEI reconstruction with other hydroclimate reconstructions from regions adjacent to our study area, including the April SPEI reconstruction in central Vietnam (Buckley et al., 2017), the March–May relative humidity (RH) reconstruction in northern Thailand (Pumijumnong et al., 2023), and the March–May PDSI reconstruction in southern Vietnam (Buckley et al., 2010). Furthermore, we evaluated the association of our reconstructed series with different climate modes, such as ENSO (Niño 3.4), Multivariate ENSO Index (MEI v2), Oceanic Niño Index (ONI), and Southern Oscillation Index (SOI). These climate modes are active due to broad-scale ocean-atmospheric circulation patterns and strongly influence the climate of both our study region and Southeast Asia.

Table 2
Calibration-verification statistics for the March–August SPEI reconstruction from 1960 to 2019.

Calibration model: $Y_{SPEI} = 2.898\ X_{RWI} - 2.772$, $p < 0.001$

Period	r	r^2	r^2_{adj}	F	SE	DW
1960–2019	0.657	0.431	0.422	44.009	0.401	1.554

(a) Leave-one-out verification

Period	r_{ver}	r^2_{ver}	ST	Pmt	RMSE	RE
1960–2019	0.630	0.397	+44/−16	5.021	0.406	0.396

(b) Split-sample calibration-verification

Verification statistics	Calibration (1960–1989)	Verification (1990–2019)	Calibration (1990–2019)	Verification (1960–1989)
r	0.660		0.673	
r^2	0.435		0.453	
r^2_{adj}	0.415		0.434	
F	21.56		23.22	
SE	0.359		0.438	
r_{ver}		0.673		0.660
r^2_{ver}		0.453		0.435
ST		+22/−8		+24/−6
RE		0.406		0.364
CE		0.382		0.324

(a) Leave-one-out (LOOV) calibration-verification statistics. (b) Split-sample calibration-verification statistics. All calibration and verification statistics were calculated with a significance level of $p < 0.001$, while the Durbin-Watson (DW) statistic was evaluated with a significance level of $p > 0.05$. SE, standard error of estimates; Pmt, product-mean test; RMSE, root-mean-square error; ST, sign test; CE, coefficient of efficiency; RE, reduction of error.

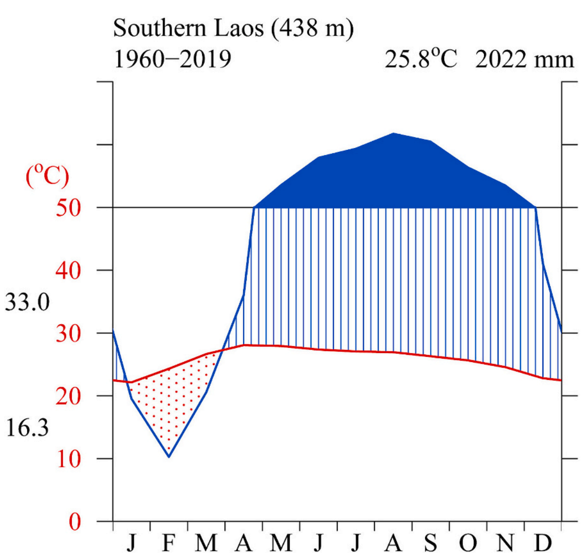

Fig. 2. The Walter-Lieth climate diagram of the study area representing the regional climate in southern Laos. The regional climate data were derived by averaging the climate data from three respective CRU grids on which the tree-ring sites are located.

3. Results

3.1. Tree-ring chronology characteristics

Three tree-ring site chronologies of *P. latteri* in southern Laos spanned 130 to 210 years (Fig. S3, Table 1): DPV (1810–2019), TX (1810–2019), and MM (1890–2019). Pine trees at the three study sites showed relatively high average growth rates (1.7 mm/year), ranging from 1.155 ± 0.603 mm/year at DPV site, 1.717 ± 0.849 mm/year at TX site, to 2.161 ± 0.987 mm/year at MM site (Table 1). Remarkably low and high growth variations have been observed since the 1970s, indicating strong fluctuations of climate conditions in southern Laos (Fig. 3a). The characteristics of SLC chronology indicated high dendroclimatic potential, i.e., Gini (0.270), SNR (23.582), Rbar (0.161) (Table 1). Due to the insufficient sample depth in the early part of the SLC chronology, the recommended EPS dropped below the threshold value (≥ 0.85) before 1885 CE (Fig. 3c), suggesting that the chronology was reliable for climate reconstruction from 1885 to 2019.

3.2. Growth-climate relationships

The radial growth of *P. latteri* at all three sites in southern Laos was negatively correlated with monthly temperatures (maximum, minimum, and mean) and positively correlated with monthly moisture availability (precipitation, SPEI, and scPDSI), particularly during the dry and wet months, where the seasonal correlation was highest during March–August for all climate variables (Fig. S4). Furthermore, the SLC chronology generally showed positive correlations with monthly, seasonal (March–August), and yearly (January–December) moisture variables (Prec, SPEI, scPDSI) and negative correlations with temperature variables (Tmx, Tmp, Tmn) (Fig. 4). Specifically, significant positive correlations ($p < 0.05$) were observed between the SLC chronology and current-year monthly moisture variables from January to October, while months in the previous year exhibited inconsistent or non-significant correlations. For seasonal moisture variables, correlations ranged from 0.515 to 0.657, and for yearly moisture, correlations ranged from 0.396 to 0.606. Among moisture variables, SPEI showed the strongest positive correlation during March–August (r = 0.657, $p < 0.001$). Conversely, significant negative correlations ($p < 0.05$) were found between the SLC chronology and monthly temperatures from January to August, with significant correlations also present in the previous year from October to December. Among temperature variables, Tmx demonstrated the strongest negative correlation ($r = -0.621$, $p < 0.001$) during March–August. Overall, the highest correlation ($r = 0.657$, $p < 0.001$) was found between the SLC chronology and March–August SPEI (Fig. 4), indicating that the radial growth of *P. latteri* trees in southern Laos is primarily limited by moisture availability during the dry-to-wet months (i.e., March–August). Correlation analysis of the SLC chronology with the first-order differences of climatic variables demonstrated consistent growth-climate relationships (Fig. S5), suggesting that the influence of autocorrelations in climate time series was minimal. The results of the moving correlation analysis revealed an increasing strength of negative temperature sensitivity in recent decades since the 1970s, but stable moisture sensitivity of tree growth over time in southern Laos (Fig. S6).

3.3. March–August SPEI reconstruction

Based on the response of *P. latteri* tree growth to various climatic variables, March–August SPEI was identified as the best candidate for reconstruction. Therefore, we constructed a linear regression model ($Y_{SPEI} = 2.898\ X_{RWI} - 2.772$) to reconstruct the regional March–August SPEI variations in southern Laos back to 1885. Y_{SPEI} represents the reconstructed March–August SPEI value, while X_{RWI} refers to the associated tree ring-width index for a given year. The reconstruction explained 43.1 % of the observed March–August SPEI variance during the calibration period 1960–2019. The Durbin-Watson statistic (1.554) is close to 2.0 (Table 2), suggesting minimal autocorrelation in the regression residuals of the calibration model. A comparison of the observed and predicted SPEI series also indicates that the reconstruction closely matches the actual March–August SPEI across both high and low frequencies (Fig. 5b). The significant sign-test (+44/−16), significant product mean test (Pmt, 5.021), smaller RMSE (0.406) compared to the SD (0.527) between the observed data and the leave-one-out estimates,

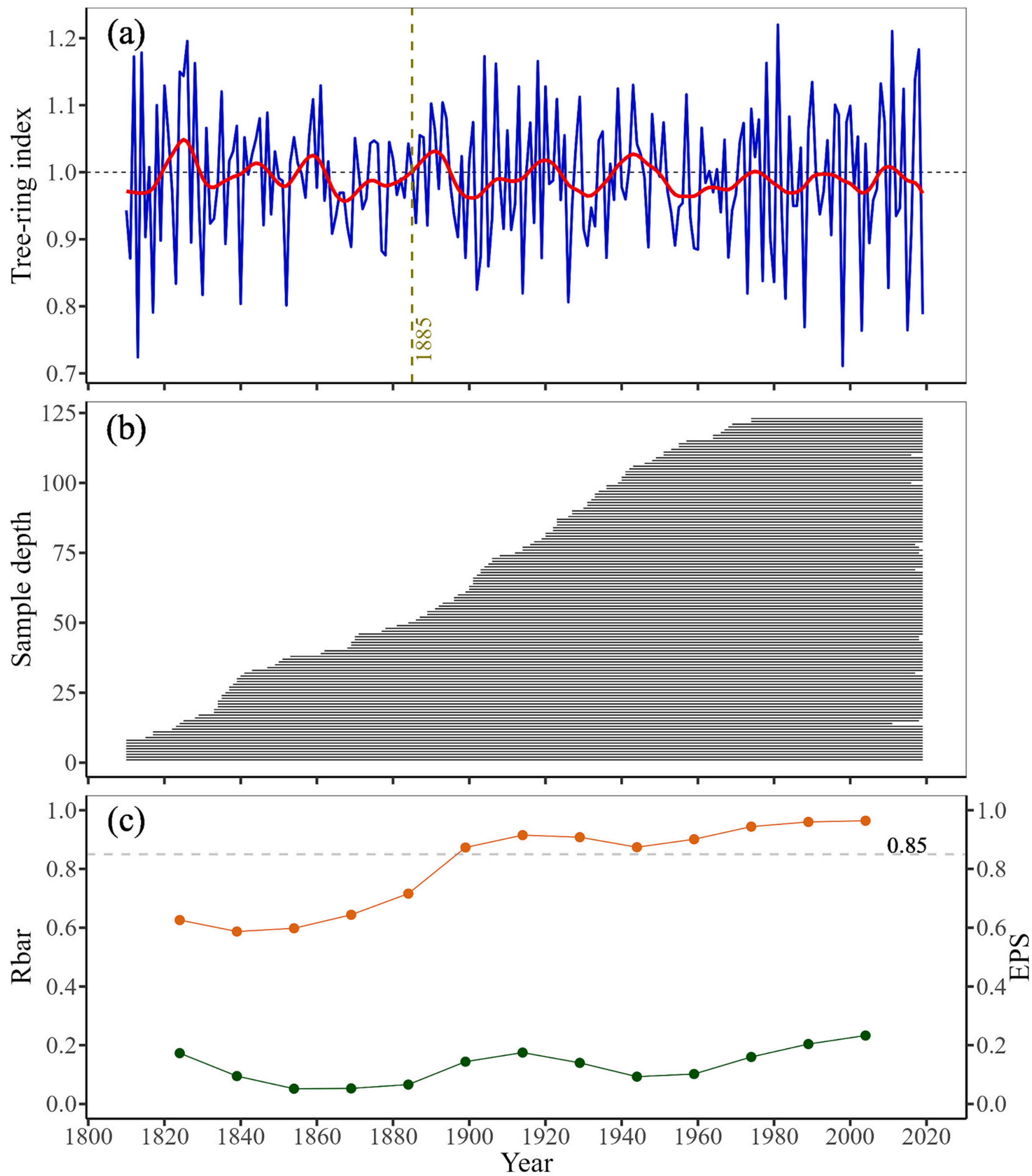

Fig. 3. Regional composite residual chronology of *Pinus latteri* in southern Laos for the period 1810–2019. (a) ring-width residual chronology (blue line) with a 15-year smoothing spline (red line), (b) number of series (horizontal grey line), and (c) expressed population signal (EPS, orange line with solid circles) and running inter-series correlation (Rbar, green line with solid circles) in a 30-year window with a 15-year overlap. (For interpretation of the references to colour in this figure legend, the reader is referred to the web version of this article.)

together confirmed the strong predictive skills of our reconstruction. The positive values of CE (0.382/0.324) and RE (0.406/0.364) in the split-sample verification (Table 2) further verified the validity and reliability of the reconstruction.

The March–August SPEI reconstruction identified distinct dry and wet periods over the last 135 years (1885–2019) in southern Laos (Fig. 5c). The mean value of our reconstructed SPEI series was 0.095 (Fig. 5c), indicating that the region experienced mild wet or near-normal moisture conditions. Our March–August SPEI reconstruction recorded eleven extremely dry and 20 dry events from 1885 to 2019 (Fig. 5c, Table S4). The extremely dry years were 1902, 1914, 1926, 1973, 1983, 1988, 1998, 2003, 2010, 2015, and 2019 (Fig. 5c, Table S4). In contrast, only seven extremely wet years and 23 wet years were identified during the past 135 years. Extremely wet years were 1904, 1907, 1918, 1978, 1981, 2011, and 2018 (Fig. 5c, Table S4). Wet episodes occurred in 1886–1895, 1906–1909, 1915–1924, 1937–1951, 1972–1978, 1989–1997, 1999–2000, 2007–2013, and 2017 (Fig. 5c, Table S4). Dry episodes were more frequent and lasted longer than wet periods. Many moderate-to-severe dry episodes were observed in 1885, 1896–1905, 1910–1914, 1925–1936, 1952–1971, 1979–1988, 1998, 2001–2006, 2014–2016, and 2018–2019 (Fig. 5c, Table S4). Notably, the frequency of extreme drought occurrence intensified in recent decades since the 1970s (Figs. 5c, 6), which coincides with anthropogenic global climate change (AghaKouchak et al., 2014; IPCC, 2023).

3.4. Spatial correlation and teleconnections

Multi-Taper spectral analysis revealed high-frequency periodicities of 2.3–3.1 years in the March–August SPEI reconstruction (Fig. 7a). Similarly, the Morlet wavelet analysis identified high-frequency cycles of 2 to 4 years, mostly in recent decades since the 1970s, as well as in the earlier period of reconstruction (Fig. 7b). The 2–4 years spectral periodicities may be associated with large-scale ocean-atmospheric circulations, mainly ENSO activities.

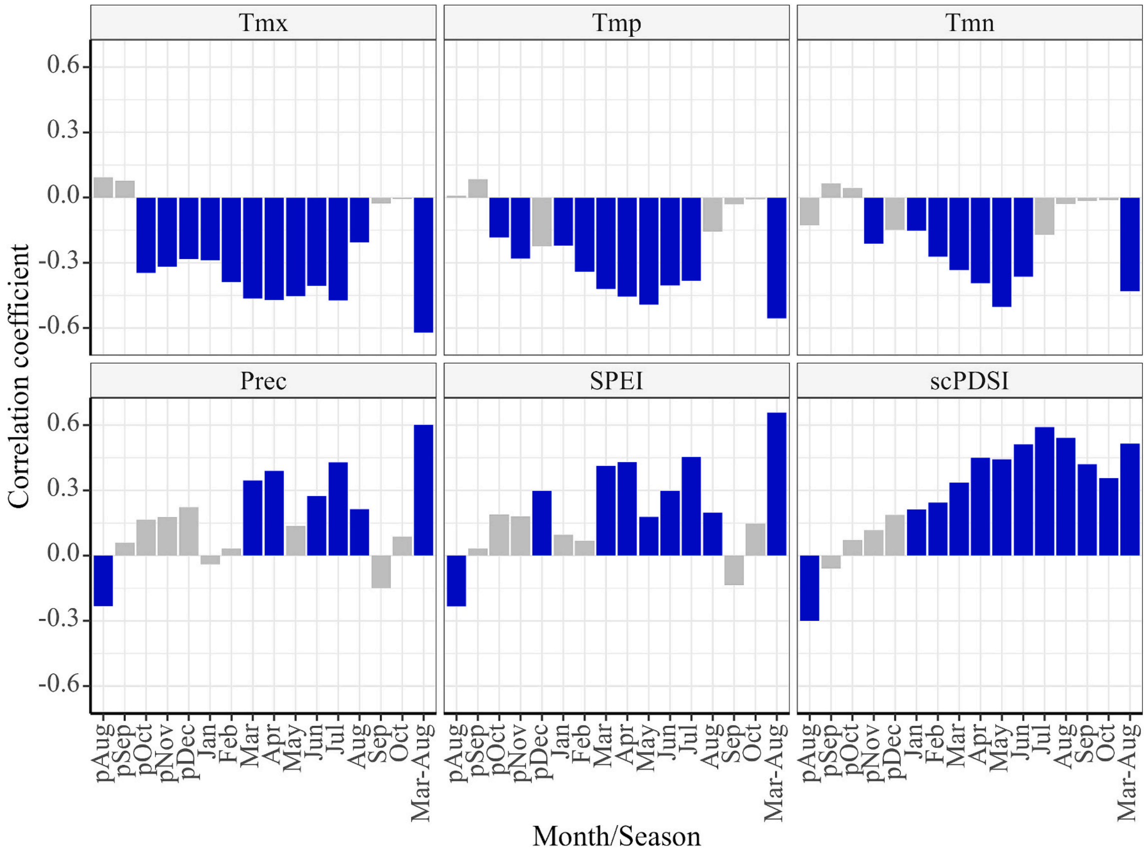

Fig. 4. Correlations between the regional composite residual chronology and monthly climate data from 1960 to 2019. Climate variables: maximum (Tmx), mean (Tmp), and minimum (Tmn) temperatures; precipitation (Prec); self-calibrated Palmer Drought Severity Index (scPDSI); one-month Standardized Precipitation-Evapotranspiration Index (SPEI). The one-month SPEI refers to the SPEI calculated over a 1-month period. Correlation coefficients with significance at $p < 0.05$ are highlighted in blue. (For interpretation of the references to colour in this figure legend, the reader is referred to the web version of this article.)

The spatial correlation of our reconstructed SPEI series with CRU maximum temperature and precipitation indicated that March–August SPEI variability in southern Laos is strongly associated with temperature and precipitation changes over the wider areas of peninsular Southeast Asia. Meanwhile, the magnitude of spatial correlations of the reconstructed SPEI with maximum temperature was highest in southern Laos and extended into neighboring regions in Vietnam and Thailand (Fig. 8b). Likewise, our drought reconstruction had a strong association with gridded precipitation in southern Laos (Fig. 8a). Furthermore, spatial correlation maps showed a very clear negative association between the reconstructed March–August SPEI and SSTs anomalies in the tropical Pacific Ocean, mostly in the Niño 3.4 region as well as in the tropical Indian Ocean, throughout the period from 1960 to 2019 (Fig. 9). Interestingly, the negative association of reconstructed March–August SPEI was higher with January–June SSTs anomalies than with March–August SSTs anomalies in the tropical Pacific Ocean (Fig. 9). Concomitantly, low moisture availability during March–August in southern Laos was associated with concurrent high SSTs in the tropical Indian Ocean, which is consistent, although a slightly higher correlation was observed with January–June SSTs anomalies (Fig. 9).

The dry-wet episodes in March–August SPEI reconstruction coincided with the dry-wet episodes in other precipitation or drought reconstructions in Southeast Asia (Fig. 10). The reconstruction also showed significant negative correlations with dominant climate indices associated with ENSO activities (Niño 3.4, ONI, and MEI) and positive correlation with SOI, especially during dry season months (Fig. S8). Similarly, a positive association of reconstructed March–August SPEI is also found with both the East Asian summer monsoon (EASM) and the South Asian summer monsoon (SASM) indices during summer months, with a positive association with EASM being much stronger than SASM (Fig. S9).

4. Discussion

4.1. Climate sensitivity of pine growth

Three site chronologies of *P. latteri* from southern Laos showed synchronous growth (Fig. S3, Table S2), indicating a shared climatic factor that constrains tree growth (Fig. S4). We observed that all site and regional composite chronologies of *P. latteri* from southern Laos showed negative correlations with higher temperatures and positive correlations with moisture variables such as precipitation, SPEI, and scPDSI, particularly from March to August (Fig. 4, Fig. S4). The highest positive relationship was observed between the regional composite chronology and March–August SPEI (Fig. 4), indicating that *P. latteri* growth in southern Laos is primarily limited by moisture availability during the dry-to-wet months (March–August), when temperatures are relatively high (Fig. 2). In tropical Southeast Asian regions, tree growth is positively associated with moisture, particularly during the dry season, where the higher temperatures further alleviate atmospheric and meteorological drought (Zuidema et al., 2022; Pumijumnong et al., 2023).

The significant positive correlations between moisture variables (precipitation, SPEI, scPDSI) and the SLC chronology suggest that moisture availability plays a crucial role in the growth of *P. latteri* in southern Laos, particularly during the critical period of cambial activity. Conversely, significant negative correlations with temperature variables (maximum, mean and minimum temperatures) imply that high

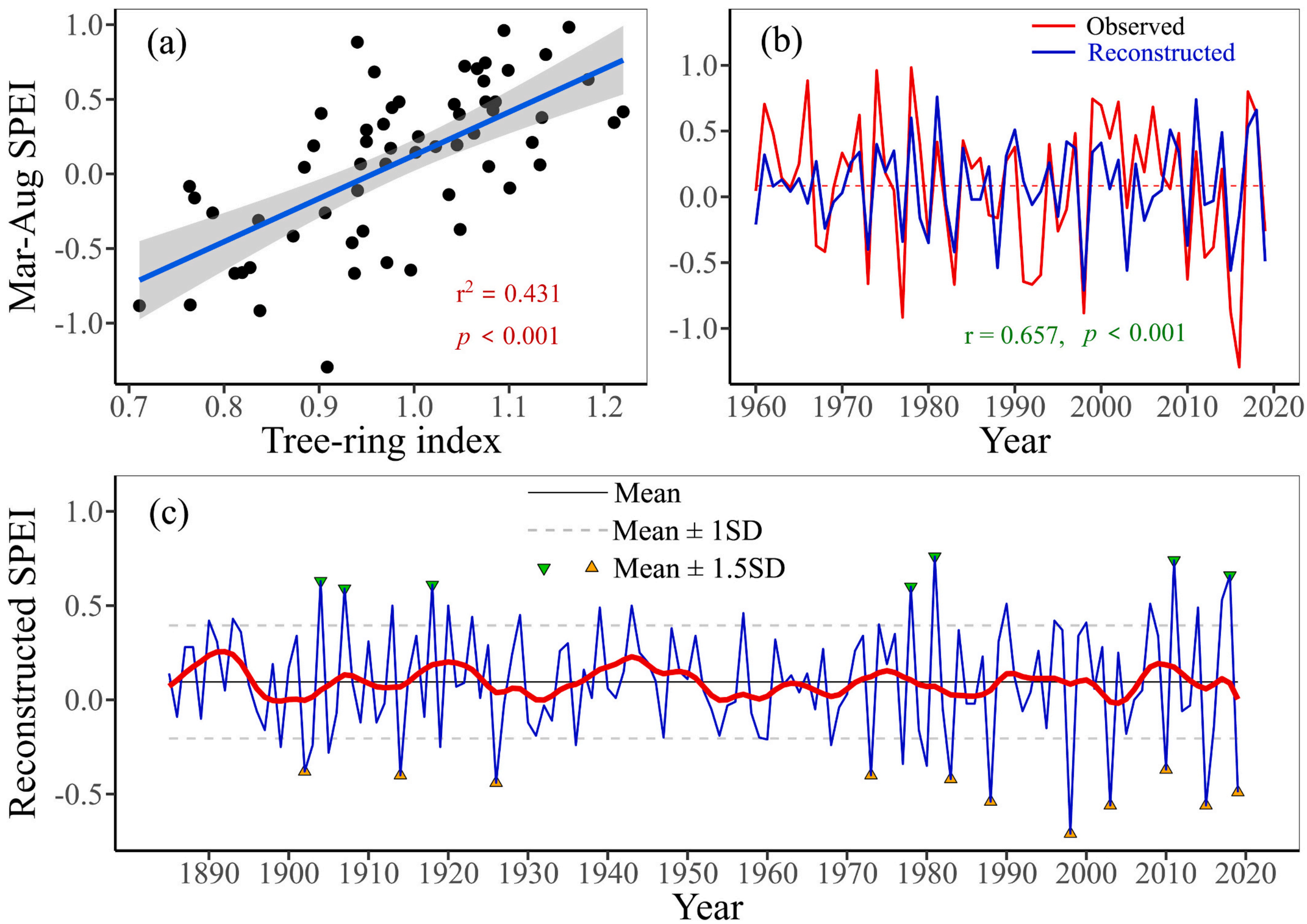

Fig. 5. March–August SPEI reconstruction derived from tree-ring composite chronology of *Pinus latteri* in southern Laos. (a) Relationship between the chronology and observed March–August SPEI. (b) Comparison of the observed March–August SPEI (red line) and the reconstructed series (blue line) from 1960 to 2019. (c) Reconstructed March–August SPEI series (blue line) with a 10-year spline filter (red line) for the period 1885–2019. The green and orange triangles denote 1.5 standard deviations (SD) above and below the long-term mean of the reconstructed series. (For interpretation of the references to colour in this figure legend, the reader is referred to the web version of this article.)

temperatures may stress *P. latteri* due to increased evapotranspiration leading to water stress. The role of seasonality is underscored by the highest positive correlation observed with SPEI during March–August, indicating that moisture during this period is essential for radial growth. While the moisture conditions of the previous year show weaker correlations with tree growth, the significant negative correlations with temperature from October to December of the previous year suggest that warm conditions before dormancy could deplete energy reserves or impact bud formation, influencing subsequent growth. During the earlier months (March–July), precipitation remains insufficient to support optimal growth in these tropical habitats due to high temperatures and potential evapotranspiration, until precipitation peaks in August (Krishnaswamy et al., 2013). Sufficient moisture supply ensures that the tree's physiological processes, such as water availability, nutrient uptake, and photosynthesis, can occur optimally. During the dry and wet months, temperatures are relatively high (peaking in April) in southern Laos (Fig. 2). High temperatures enhance the rate of evapotranspiration, resulting in substantial soil moisture stress, tree water deficit, and limitation of cambium activity (Bonan, 2008; Corlett, 2016; Pumijumnong and Palakit, 2020). Additionally, high temperatures may reduce carbon dioxide uptake, prompting plants to close stomata, decrease biological enzyme activity, and subsequently hinder photosynthesis and the accumulation of photosynthetic products (Keenan et al., 2013; Dai, 2019).

Consistent with our findings, Rakthai et al. (2020) reported that the growth of *P. latteri* from northern/northeastern Thailand was significantly positively correlated with moisture variables (precipitation, relative humidity and scPDSI) during April to June, and negative relationships with temperatures from April to August. Similarly, the radial growth of *P. kesiya* and *P. latteri* showed negative associations with temperatures from March to May in northwestern Thailand (Pumijumnong and Eckstein, 2010). In northern Thailand, *P. latteri* growth exhibited a positive correlation with relative humidity from March to May (Pumijumnong et al., 2023) and a negative relationship with August temperature (Naumthong et al., 2021). The radial growth of *P. smithiana* in the Himalayan region is predominantly constrained by moisture availability from March to May (Panthi et al., 2017), while *P. wallichiana* shows a positive correlation with scPDSI and a negative correlation with temperature during February to August (Gaire et al., 2019). Pumijumnong and Wanyaphet (2006) reported that the cambium of *P. latteri* starts to grow in April to May and progresses throughout the rainy season in northern Thailand. The cambial activity of *P. latteri* and *P. kesiya* from northern Thailand began in May, and their radial growth had positive correlations with April–May rainfall and negative relationships with temperatures during dry to wet months (Pumijumnong et al., 2021).

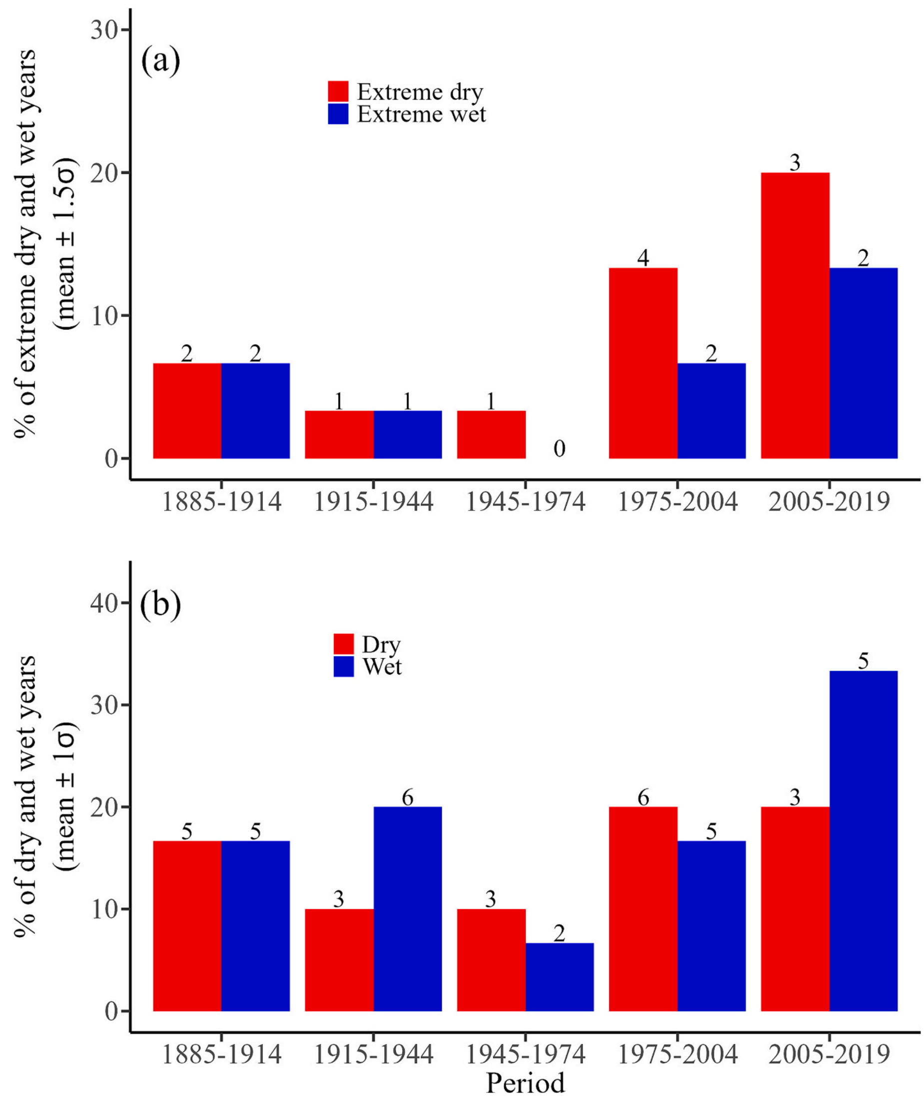

Fig. 6. Percentage of extreme dry/wet years (a) and percentages of dry/wet years (b) in March–August SPEI reconstruction, analyzed over a 30-year window from 1885 to 2019. The numbers indicate the count of events during the respective periods. The period 2005–2019 spans only 15 years.

4.2. Drought history in Laos

Our reconstructed March–August SPEI series has identified several dry and wet episodes in southern Laos over the past 135 years (Table S4; Fig. 10). Notably, prolonged droughts occurred on a decadal scale during 1896–1905, 1925–1936, 1952–1971, and 1979–1988. These findings are consistent with drought and relative humidity reconstructions from neighboring regions in Southeast Asia (Fig. 10; Buckley et al., 2010, 2017; Pumijumnong et al., 2023). Our reconstruction aligns with the drought periods in central Vietnam, specifically 1896–1905, 1910–1914, 1956–1962, 1968–1971, and 2005–2006, as reported by the April SPEI reconstruction (Buckley et al., 2017; Fig. 10b). It also matches drought episodes in southern Vietnam, including 1885, 1896–1905, 1911–1914, 1933–1936, 1957–1964, 1968–1970, 1979–1985, and 2002–2005, recorded by the March–May PDSI reconstruction (Buckley et al., 2010; Fig. 10d). Additionally, our reconstruction corresponds well with dry periods identified in northern Thailand, such as 1885, 1900–1905, 1930–1936, 1956–1970, 1979–1988, 2004–2006, 2016, as well as wet periods like 1907–1909, 1915–1918, 1920–1922, 1940–1951, 1972–1977, 1994–1997, 1999–2000, 2011–2013 (Pumijumnong et al., 2023; Fig. 10c). Our findings also coincided with most drought periods in southwest China, including 1896–1902, 1910–1914, 1925–1936, 1953–1963, 1968–1971, 1982–1987, and 2018–2019, as revealed by the March–June SPEI reconstruction (Yin et al., 2023). Furthermore, our SPEI series captured significant dry years in Myanmar, such as 1899, 1926, 1977, 1980, 1983, and 2010, derived from the teak tree ring-based scPDSI reconstruction (Zaw et al., 2020). The year 2010 was also identified as a drought year in Myanmar (Zaw et al., 2020), the central Himalayas (Panthi et al., 2017; Gaire et al., 2019), and southwest China (Yin et al., 2023). Our reconstruction detected two dry episodes, 1955–1960 and 1979–1988, which were also recorded in the Monsoon Asia Drought Atlas reported by Cook et al. (2010). Discrepancies between our findings and other hydroclimate reconstructions might arise from differences in tree species, sampling locations, climatic variables, and the season reconstructed (Buckley et al., 2017; Zaw et al., 2020; Yin et al., 2023).

Our March–August drought reconstruction in southern Laos shows an increasing frequency of extreme dry and wet years since the 1970s (Fig. 6). The increasing variability in droughts is likely linked to regional and global warming, which significantly alters the frequency of extreme events (Trenberth et al., 2004; IPCC, 2023). Changes in global circulation pattern are expected to cause widespread increases in droughts and shifts in drought regimes (Dai, 2010). Climate change, characterized by rising temperatures, shifting rainfall patterns, and increased tropical cyclones, leads to extreme events like floods and droughts, which are major hazards in Laos (UNDRR, 2013; Miyan, 2015). Areas receiving

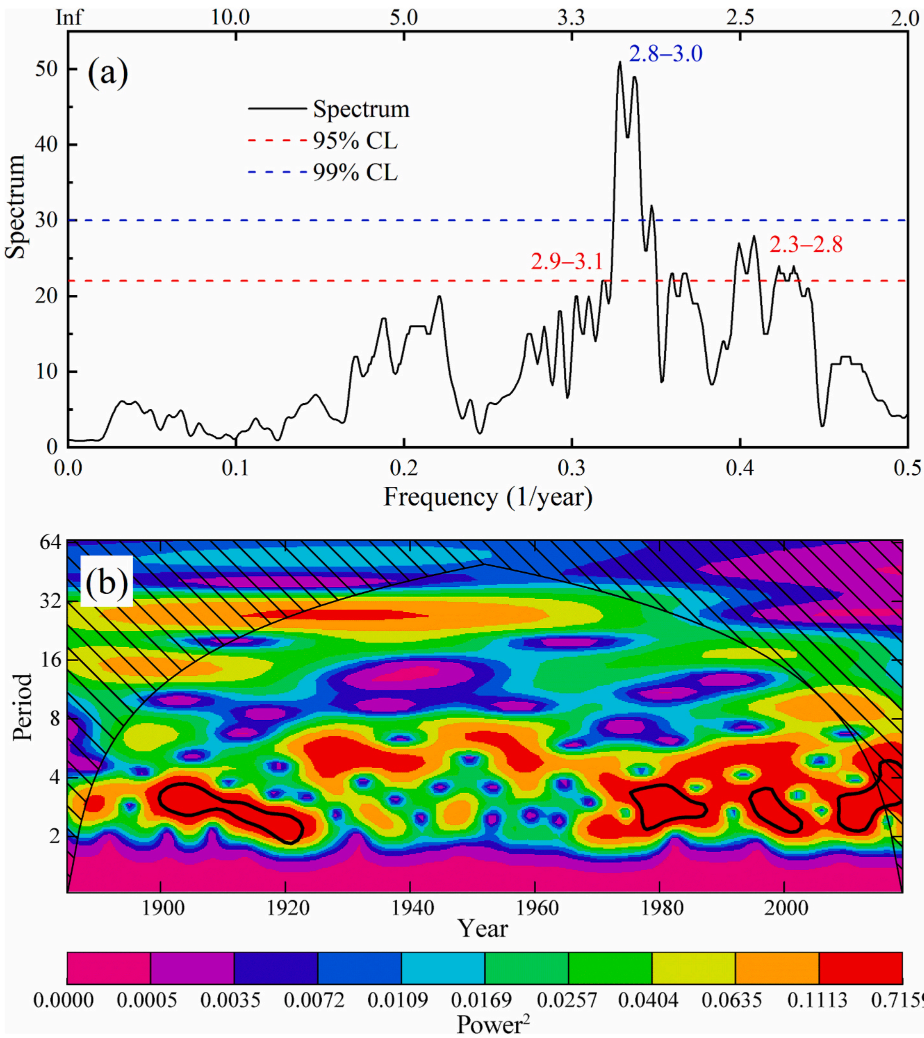

Fig. 7. Spectral analysis of the reconstructed March–August SPEI series for southern Laos from 1885 to 2019. (a) Power spectrum of the reconstructed March–August SPEI, with confidence levels at 95 % (red dashed line) and 99 % (blue dashed line). (b) Morlet wavelet spectrum of the reconstructed March–August SPEI with the 95 % confidence level indicated by the black contour. (For interpretation of the references to colour in this figure legend, the reader is referred to the web version of this article.)

less than 2000 mm of annual rainfall are drought-sensitive, while more than 200 mm of rainfall in two days can lead to floods (UNDRR, 2013). Our tree-ring sampling sites, located at low latitudes and elevations (Table 1), have recently experienced rising temperatures and high inter-annual precipitation fluctuations (Fig. S1). These changes contribute to increased evapotranspiration and decreased soil moisture, which in turn affect tree growth and water-use efficiency, ultimately leading to drought conditions (Betts et al., 2007; Corlett, 2016).

Drought events are often influenced by fluctuations in the monsoon system, variability due to ENSO, and the impacts of climate change. The El Niño phase of ENSO tends to reduce rainfall and contribute to drier-than-average conditions in Southeast Asia, including Laos (Phan-Van et al., 2022). The inter-annual variability of the monsoon also plays a crucial role, affecting both the timing and intensity of rainfall, which impacts water availability for agriculture and natural ecosystems (Räsänen et al., 2016; Mekong River Commission, 2019). Additionally, climate change effects, such as rising temperatures and increased evaporation rates, exacerbate drought risk, especially during dry season (IPCC, 2023).

Droughts are among the most frequent and destructive disasters in Laos. Laos is extremely susceptible to the effects of climate change and has faced increasingly frequent and severe floods and droughts over the last three decades (Maniphousay, 2021). Extreme climate events are expected to increase in both frequency and intensity, leading to a rise in climate-related hazards (Lao PDR, 2013; Zhang et al., 2020). Drought conditions have been observed in Laos since the 1980s. From 1966 to 2008, there have been nine recorded drought disasters, with the cost of damages rising in the past decade. The droughts of 1988 and 1989 were particularly severe in southern Laos, resulting in damages of up to 40 million and 20 million US dollars, respectively (ADPC, 2010). Miyan (2015) reported that moderate to severe droughts resulted in significant impacts on lives and property in Laos during the years 1961, 1966, 1971, 1978, 1984, 1994–1996, and 2009. The historical record during the period 1966–2009 indicates that Laos faces an average of 1.5 severe droughts and floods annually (GFDRR, 2011).

4.3. Possible teleconnections

Ocean-atmospheric circulation significantly affects hydroclimate variability (Bigg et al., 2003; Räsänen et al., 2016; Zaw et al., 2020, 2021; Pumijumnong et al., 2023). Our analysis revealed high-frequency spectral peaks within the periodicities of 2.3 to 3.1 years (Fig. 7a) and cycles ranging from 2 to 4 years (Fig. 7b), suggesting a possible link between regional drought conditions and large-scale ocean-atmospheric circulations. Many studies report that these high-frequency cycles (ranging from 2 to 8 years) often indicate the influence of ENSO on

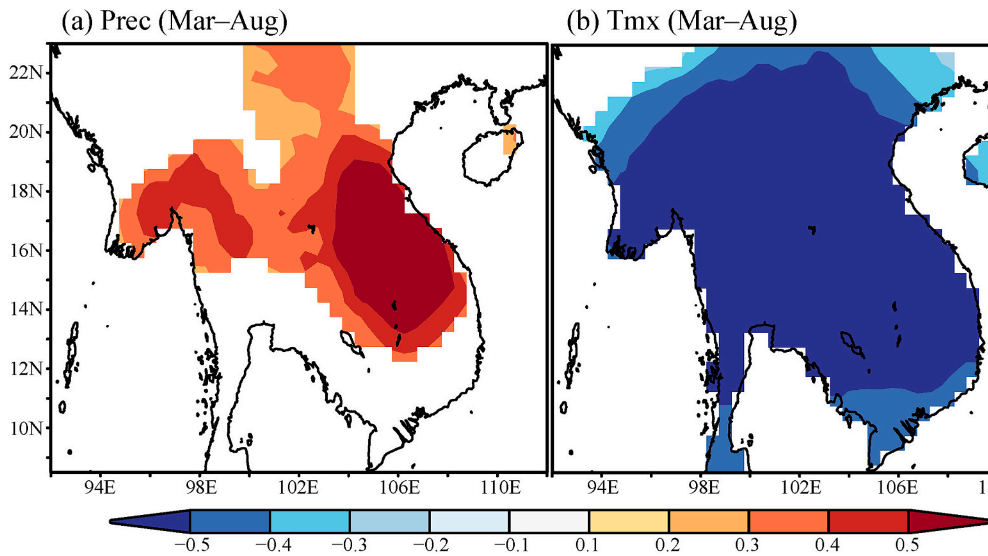

Fig. 8. Spatial correlation of the reconstructed March–August SPEI series with (a) gridded CRU precipitation and (b) gridded maximum temperature. Spatial correlations were calculated at 0.5° spatial resolution via the KNMI climate explorer from 1960 to 2019. The colour bar indicates the range of correlation coefficients. Only significant values ($p < 0.05$) are shown.

regional climates (McPhaden et al., 2006; Sano et al., 2009, 2012; Deser et al., 2010; Buckley et al., 2017; Domeisen et al., 2019). However, the similarity of these periodicities to ENSO-related cycles is noteworthy, it does not confirm a direct connection based solely on spectral analysis.

Furthermore, our reconstructed series showed significant correlations with sea surface temperatures (SSTs) in both the tropical Pacific and Indian oceans (Fig. 9). There are significant negative relationships between SSTs and drought/precipitation variability in Myanmar (Zaw et al., 2020, 2021). Strong negative relationships with high SSTs in the tropical Pacific Ocean were observed, with a lagged effect of two months (Fig. 9a). This lagged effect is also evident when comparing the reconstructed March–August SPEI with the running three-month Oceanic Niño Index (ONI), where most of the extreme drought years showed a lagged relationship (Fig. S7). The correlations between our reconstructed SPEI series and monthly oceanic indices, including Niño3.4 anomalies, ONI, MEI, and SOI, confirm these findings (Fig. S8).

Drought events are often driven by large-scale atmospheric and oceanic processes, with El Niño events frequently leading to dry conditions across Southeast Asia, including Laos. Trenberth et al. (2014) reported that droughts in Australia, Southeast Asia, Africa, and northeastern Brazil are associated with the offshore displacement of primary rainfall systems over the tropical Pacific during El Niño periods. The influence of ENSO on drought patterns varies over time and across different regions, as different ENSO events produce different precipitation anomalies (Räsänen et al., 2016; Yao et al., 2019). During El Niño phases, the anomalous drought conditions in Southeast Asia often coincide with a weakened monsoon circulation over the Indian subcontinent and Southeast Asia (Ummenhofer et al., 2013). This weakened monsoon is frequently accompanied by anomalous subsidence over monsoon Asia and a reduction in moisture flux. Additionally, when an Indian Ocean Dipole (IOD) event occurs alongside El Niño, severe drought conditions across Southeast Asia are more likely due to the compounded effect of a weakened South Asian monsoon. A positive IOD phase, which suppresses monsoon rainfall, results in anomalous cooling in the eastern Indian Ocean and warming in the western Indian Ocean. This temperature imbalance shifts the normal convection zone over the eastern Indian Ocean warm pool westward, further contributing drought conditions (Sein and Zhi, 2016).

We found a significant negative correlation between our reconstructed SPEI series and high SSTs in the tropical Pacific and Indian oceans during March to August (Fig. 9). Elevated SSTs in the Pacific Ocean appear to exert a substantial influence on dry-to-wet season precipitation and moisture conditions in southern Laos. Xu et al. (2015) found that canonical El Niño events are characterized by extremely warm SSTs in the eastern equatorial Pacific Ocean. Our reconstructed drought series also has significant positive correlations with East Asia Summer Monsoon Index (EASMI) (Fig. S9). Typically, higher SSTs in the Indian Ocean directly influence the Indian summer monsoon's effectiveness across Southeast Asia (Wang et al., 2022; Weldeab et al., 2022). The observed correlations between our SPEI reconstruction and SSTs in the Indian and Pacific regions (Fig. 9) suggest that droughts in southern Laos may be influenced by a combination of warmer temperatures and reduced moisture influx associated with SSTs anomalies from both oceanic domains (Cherchi and Navarra, 2012; Yin et al., 2022). Specifically, we identified moderate to strong correlations with SSTs in the southeastern equatorial Indian ocean (DMI-East), the western equatorial Indian ocean (DMI-West), and the Bay of Bengal, indicating the influence of both the Indian Ocean Dipole (IOD) and ENSO on seasonal drought variability (Yin et al., 2022).

ENSO strongly influences inter-annual variability in tropical ocean-atmosphere systems, significantly affecting Asian monsoon regions (McPhaden et al., 2006). El Niño events can trigger widespread severe droughts in the Asian monsoon region over inter-annual to decadal timescales (Dai and Wigley, 2000; Buckley et al., 2010; Cook et al., 2010; Räsänen et al., 2016; Wang et al., 2022). D'Arrigo et al. (2013) highlighted that El Niño events are associated with drought variability in Myanmar due to the eastward shift of the Walker circulation. Characterized by warmer conditions, El Niño events typically lead to reduced early monsoon rainfall and a decrease the radial growth of *F. hodginsii*, while La Niña events, associated with cooler conditions, generally bring increased moisture during the early monsoon season, enhancing tree growth (Buckley et al., 2017). Although the Asian Summer Monsoon primarily drives rainfall in our study region (Shekhar et al., 2022), the influence of ENSO is still apparent. Xu et al. (2011) analyzed stable oxygen isotopes in tree rings of *F. hodginsii*, demonstrating the relationship between ENSO and hydroclimate variability in northern Vietnam and Laos. Recent studies have reported strong connections between ENSO and droughts, observed spatially and temporally across the Mekong River Basin (Nguyen et al., 2023; Fan et al., 2024).

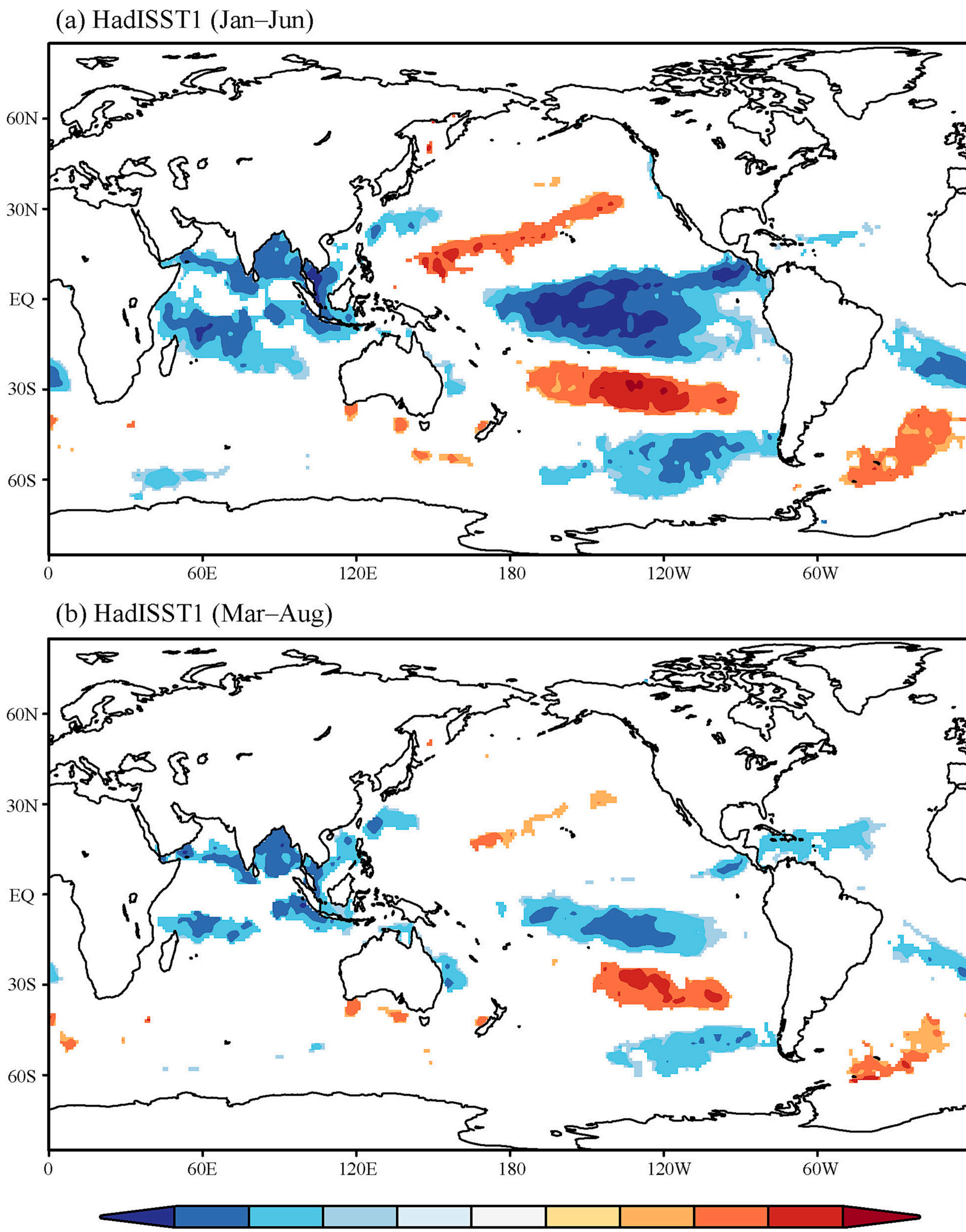

Fig. 9. Spatial correlation analysis of the reconstructed March–August SPEI series with sea surface temperatures (HadISSTs) during (a) January–June (2-month lag) and (b) March–August (concurrent). Spatial correlations were calculated at 0.5° spatial resolution via the KNMI climate explorer from 1960 to 2019. The colour bar indicates the range of correlation coefficients. Only significant values ($p < 0.05$) are shown.

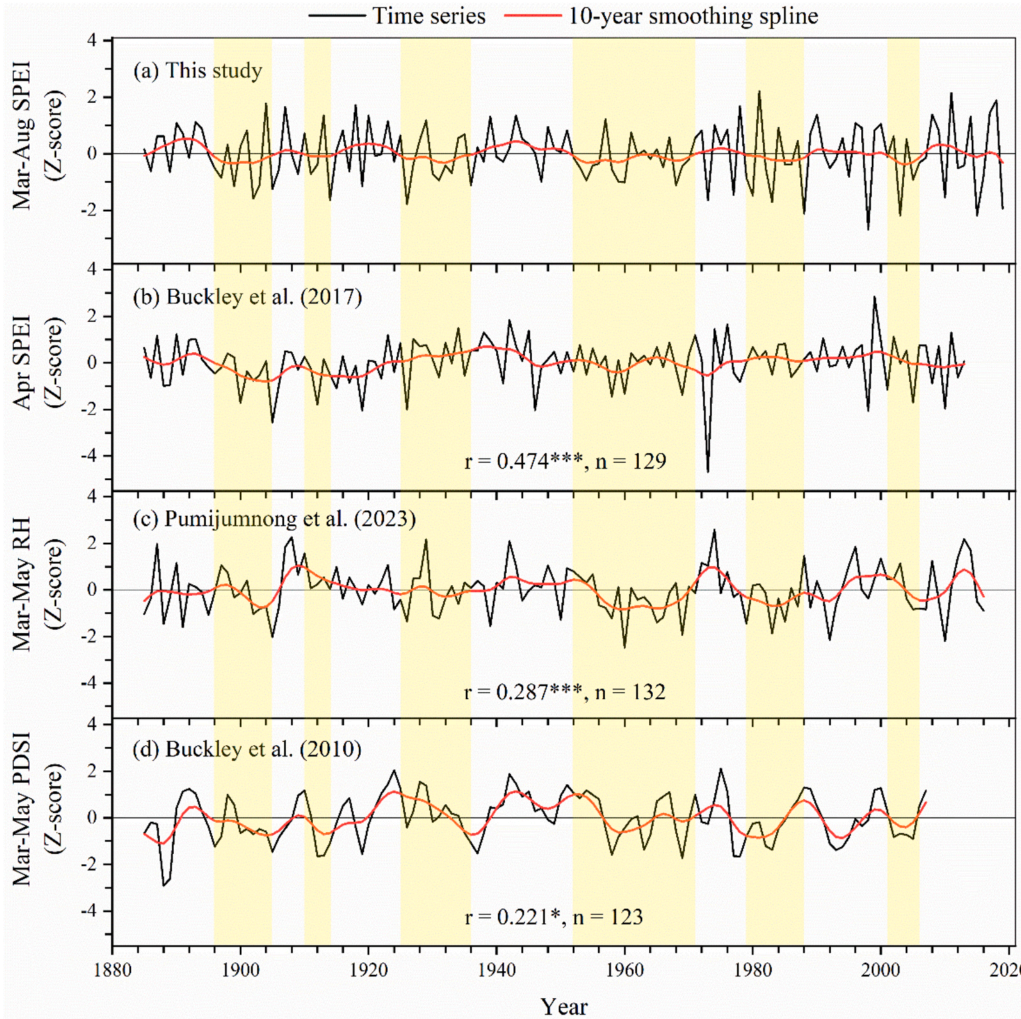

Fig. 10. Comparisons of the March–August SPEI reconstruction in southern Laos (a, this study) with other hydroclimatic reconstructions from nearby regions. (b) April SPEI reconstruction from central Vietnam (Buckley et al., 2017); (c) March–May RH reconstruction from northern Thailand (Pumijumnong et al., 2023); (d) March–May PDSI reconstruction from southern Vietnam (Buckley et al., 2010). Correlation coefficients (r) between the reconstructed SPEI series from the present study and other series for their overlapping periods are displayed. To facilitate visual comparison, all series were standardized to *Z*-scores. The black line (horizontal) represents the mean of each series. The yellow shadings (vertical) highlight the dry periods identified in this study, using a 10-year smoothing spline. (For interpretation of the references to colour in this figure legend, the reader is referred to the web version of this article.)

5. Conclusions

We developed a new regional composite chronology of *P. latteri* trees from three sites in southern Laos. Our analysis indicated that the growth of *P. latteri* was primarily constrained by moisture availability from March to August. We reconstructed the March–August SPEI for southern Laos covering the period 1885–2019, which showed variations in drought across both inter-annual and inter-decadal scales, identifying eleven extreme dry years and seven extreme wet years. Notably, the recent decades since the 1970s have witnessed an increase in extreme dry and wet events, possibly linked to ENSO activities. Hydroclimate variability in southern Laos is influenced by ocean-atmospheric circulations, particularly due to SSTs anomalies in both the tropical Pacific and Indian oceans. Our findings suggest that the rising occurrence of extreme drought events, exacerbated by global warming, may lead to more intense meteorological droughts with adverse effects on society and forest ecosystems. Consequently, it is imperative to implement mitigation strategies to address these escalating meteorological challenges. We recommend expanding the tree-ring network to enhance spatial and temporal coverage of climate proxies in Southeast Asia regions. Furthermore, comprehensive observations combining high-resolution dendrometers with cambial phenology can offer valuable insights into how different species physiologically respond to changing environmental conditions.

CRediT authorship contribution statement

Nakhonekham Xaybouangeun: Writing – review & editing, Writing – original draft, Visualization, Methodology, Formal analysis, Data curation, Conceptualization. **Zaw Zaw:** Writing – review & editing, Writing – original draft, Visualization, Supervision, Software, Methodology, Formal analysis, Data curation, Conceptualization. **Rao-Qiong Yang:** Writing – review & editing, Software. **Shankar Panthi:** Writing – review & editing, Writing – original draft, Software, Formal analysis, Conceptualization. **Dao-Xiong Gao:** Writing – review & editing. **Viengsy Paothor:** Writing – review & editing, Resources. **Ze-Xin Fan:** Writing – review & editing, Supervision, Software, Resources, Methodology, Investigation, Funding acquisition, Formal analysis, Data curation, Conceptualization.

Declaration of competing interest

The authors declare that they have no known competing financial interests or personal relationships that could have appeared to influence the work reported in this paper.

Data availability

Data will be made available on request.

Acknowledgments

We thank the Department of Forestry, Ministry of Agriculture and Forestry of Laos, for granting permission for tree-ring sampling, and all members for their field sampling assistance. The meteorological data of the Pakse, Salavan, and Savannakhet stations were obtained from the Department of Meteorology and Hydrology, Ministry of Natural Resources and Environment of Laos. We thank Prof. Brendan M. Buckley and Prof. Nathsuda Pumijumnong for sharing tree-ring reconstruction data. This study was financially funded by the National Natural Science Foundation of China (NSFC, 32471678, 31770533) and the West Light Talent Program of the Chinese Academy of Science (xbzg-zdsys-202218). N. X. gratefully acknowledges the XTBG-CAS for supporting his Ph.D. scholarship. Z. Z. was supported by the Research Fund for International Young Scientists from the National Natural Science Foundation of China (NSFC, 32250410306), the 2022 Zhihui-Yunnan Grant for Young Scientists (202303AM140020), and the Open Fund of Key Laboratory of Tropical Forest Ecology of Chinese Academy of Sciences. *Z*-X. F. was also supported by the Ten Thousand Talent Project of Yunnan Province (YNWR-QNBJ-2019–190).

Appendix A. Supplementary data

Supplementary data to this article can be found online at https://doi.org/10.1016/j.palaeo.2024.112595.

References

ADPC, 2010. Mainstreaming Disaster Risk Reduction. Asian Disaster Preparedness Centre, Bangkok, Thailand.

AghaKouchak, A., Cheng, L., Mazdiyasni, O., Farahmand, A., 2014. Global warming and changes in risk of concurrent climate extremes: Insights from the 2014 California drought. Geophys. Res. Lett. 41 (24), 8847–8852. https://doi.org/10.1002/2014gl062308.

Averyanov, L.V., Nguyen, T.H., Sinh, K.N., Pham, V., Lamxay, V., Bounphanmy, S., Lorphengsy, S., Phan, L.K., Lanorsavanh, S., Chantthavongsa, K., 2014. Gymnosperms of Laos. Nord. J. Bot. 32 (6), 765–805. https://doi.org/10.1111/njb.00498.

Barichivich, J., Osborn, T., Harris, I., Van Der Schrier, G., Jones, P., 2023. Global climate. Bull. Am. Meteorol. Soc. 104 (9), S11–S145. https://doi.org/10.1175/bams-d-23-0090.1.

Beguería, S., Vicente Serrano, S.M., Reig-Gracia, F., Latorre Garcés, B., 2023. SPEIbase v. 2.9 [Dataset], DIGITAL.CSIC, Version 2.9. https://doi.org/10.20350/digitalCSIC/15470.

Betts, R.A., Boucher, O., Collins, M., Cox, P.M., Falloon, P.D., Gedney, N., Hemming, D. L., Huntingford, C., Jones, C.D., Sexton, D.M.H., Webb, M.J., 2007. Projected increase in continental runoff due to plant responses to increasing carbon dioxide. Nature 448 (7157), 1037–1041. https://doi.org/10.1038/nature06045.

Bigg, G.R., Jickells, T.D., Liss, P.S., Osborn, T.J., 2003. The role of the oceans in climate. Int. J. Climatol. 23 (10), 1127–1159. https://doi.org/10.1002/joc.926.

Bonan, G.B., 2008. Forests and climate change: Forcings, feedbacks, and the climate benefits of forests. Science 320 (5882), 1444–1449. https://doi.org/10.1126/science.1155121.

Buckley, B.M., Duangsathaporn, K., Palakit, K., Butler, S., Syhapanya, V., Xaybouangeun, N., 2007. Analyses of growth rings of *Pinus merkusii* from Lao P.D.R. For. Ecol. Manag. 253 (1–3), 120–127. https://doi.org/10.1016/j.foreco.2007.07.018.

Buckley, B.M., Anchukaitis, K.J., Penny, D., Fletcher, R., Cook, E.R., Sano, M., Nam, L.C., Wichienkeeo, A., Minh, T.T., Hong, T.M., 2010. Climate as a contributing factor in the demise of Angkor, Cambodia. Proc. Natl. Acad. Sci. USA 107 (15), 6748–6752. https://doi.org/10.1073/pnas.0910827107.

Buckley, B.M., Stahle, D.K., Luu, H.T., Wang, S.Y.S., Nguyen, T.Q.T., Thomas, P., Le, C. N., Ton, T.M., Bui, H., Nguyen, V.T., 2017. Central Vietnam climate over the past five centuries from cypress tree rings. Clim. Dyn. 48 (11–12), 3707–3723. https://doi.org/10.1007/s00382-016-3297-y.

Bunn, A.G., 2008. A dendrochronology program library in R (dplR). Dendrochronologia 26 (2), 115–124. https://doi.org/10.1016/j.dendro.2008.01.002.

Cherchi, A., Navarra, A., 2012. Influence of ENSO and of the Indian Ocean Dipole on the Indian summer monsoon variability. Clim. Dyn. 41 (1), 81–103. https://doi.org/10.1007/s00382-012-1602-y.

Cook, E.R., Kairiukstis, L.A., 1990. Methods of Dendrochronology. Kluwer Academic Press, Netherlands. https://doi.org/10.1007/978-94-015-7879-0.

Cook, E.R., Peters, K., 1997. Calculating unbiased tree-ring indices for the study of climatic and environmental change. Holocene 7 (3), 361–370. https://doi.org/10.1177/095968369700700314.

Cook, E.R., Anchukaitis, K.J., Buckley, B.M., D'Arrigo, R.D., Jacoby, G.C., Wright, W.E., 2010. Asian monsoon failure and megadrought during the last millennium. Science 328 (5977), 486–489. https://doi.org/10.1126/science.1185188.

Corlett, R.T., 2016. The Impacts of droughts in tropical forests. Trends Plant Sci. 21 (7), 584–593. https://doi.org/10.1016/j.tplants.2016.02.003.

Dai, A., 2010. Drought under global warming: a review. Wiley Interdiscip. Rev. Clim. Chang. 2 (1), 45–65. https://doi.org/10.1002/wcc.81.

Dai, W., 2019. Stress Physiology of Woody Plants. CRC Press eBooks. https://doi.org/10.1201/9780429190476.

Dai, A., Wigley, T.M.L., 2000. Global patterns of ENSO-induced precipitation. Geophys. Res. Lett. 27 (9), 1283–1286. https://doi.org/10.1029/1999gl011140.

D'Arrigo, R., Palmer, J., Ummenhofer, C., Kyaw, N., Krusic, P., 2013. Myanmar monsoon drought variability inferred by tree rings over the past 300 years: linkages to ENSO. PAGES News 21 (2), 50–51. https://doi.org/10.22498/pages.21.2.50.

Deser, C., Alexander, M.A., Xie, S.P., Phillips, A.S., 2010. Sea surface temperature variability: patterns and mechanisms. Annu. Rev. Mar. Sci. 2 (1), 115–143. https://doi.org/10.1146/annurev-marine-120408-151453.

Domeisen, D.I., Garfinkel, C.I., Butler, A.H., 2019. The teleconnection of El Niño Southern Oscillation to the stratosphere. Rev. Geophys. 57 (1), 5–47. https://doi.org/10.1029/2018rg000596.

Doughty, C.E., Metcalfe, D.B., Girardin, C.A.J., Amézquita, F.F., Cabrera, D.G., Huasco, W.H., Malhi, Y., 2015. Drought impact on forest carbon dynamics and fluxes in Amazonia. Nature 519 (7541), 78–82. https://doi.org/10.1038/nature14213.

Eslamian, S., Ostad-Ali-Askari, K., Singh, V., Dalezios, N., Ghane, M., Yihdego, Y., Matouq, M., 2017. A review of drought indices. Int. J. Construct. Res. Civ. Eng. 3 (4). https://doi.org/10.20431/2454-8693.0304005.

Estoque, R.C., Ooba, M., Avitabile, V., Hijioka, Y., DasGupta, R., Togawa, T., Murayama, Y., 2019. The future of Southeast Asia's forests. Nat. Commun. 10 (1). https://doi.org/10.1038/s41467-019-09646-4.

Fan, L., Wang, Y., Cao, C., Chen, W., 2024. Teleconnections of atmospheric circulations to meteorological drought in the Lancang-Mekong River Basin. Atmosphere 15 (1), 89. https://doi.org/10.3390/atmos15010089.

FAO, 2020. Global Forest Resources Assessment 2020—Key findings. Rome. https://doi.org/10.4060/ca8753en.

FAO, MONRE, MAF, 2022. Climatology and Agroclimatology Atlas of the Lao People's Democratic Republic. Vientiane. https://doi.org/10.4060/cb9713en.

Fritts, H.C., 1976. Tree Rings and Climate. Academic Press, London, New York, San Francisco.

Gaire, N.P., Dhakal, Y.R., Shah, S.K., Fan, Z.X., Bräuning, A., Thapa, U.K., Bhandari, S., Aryal, S., Bhuju, D.R., 2019. Drought (scPDSI) reconstruction of trans-Himalayan region of central Himalaya using *Pinus wallichiana* tree-rings. Palaeogeogr. Palaeoclimatol. Palaeoecol. 514, 251–264. https://doi.org/10.1016/j.palaeo.2018.10.026.

GFDRR, 2011. Typhoon Haima in the Lao PDR: Joint Damage, Losses and Needs Assessment. Retrieved from. https://www.gfdrr.org/sites/default/files/Haima_JDLNA_Report.pdf.

Grinsted, A., Moore, J.C., Jevrejeva, S., 2004. Application of the cross wavelet transform and wavelet coherence to geophysical time series. Nonlinear Process. Geophys. 11 (5/6), 561–566. https://doi.org/10.5194/npg-11-561-2004.

Guo, H., Bao, A., Liu, T., Ndayisaba, F., He, D., Kurban, A., De Maeyer, P., 2017. Meteorological drought analysis in the lower Mekong Basin using satellite-based long-term CHIRPS Product. Sustainability 9 (6), 901. https://doi.org/10.3390/su9060901.

Hartmann, H., Bastos, A., Das, A.J., Esquivel-Muelbert, A., Hammond, W.M., Martínez-Vilalta, J., McDowell, N.G., Powers, J.S., Pugh, T.A.M., Ruthrof, K.X., Allen, C.D., 2022. Climate Change risks to Global Forest Health: Emergence of Unexpected events of Elevated tree Mortality Worldwide. Annu. Rev. Plant Biol. 73 (1), 673–702. https://doi.org/10.1146/annurev-arplant-102820-012804.

Holmes, R.L., 1983. Computer-assisted quality control in tree-ring dating and measurement. Tree-Ring Bull 43 (1), 69–78. https://arizona.openrepository.com/handle/10150/261223.

IPCC. (2023). Climate Change 2023: Synthesis Report. Contribution of Working groups I, II and III to the Sixth Assessment Report of the Intergovernmental Panel on climate Change [Core writing Team, H. Lee and J. Romero (eds.)]. IPCC, Geneva, Switzerland, pp. 35-115. Doi:10.59327/ipcc/ar6-9789291691647.

Kang, H., Sridhar, V., 2020. A near-term drought assessment using hydrological and climate forecasting in the Mekong River Basin. Int. J. Climatol. 41 (S1). https://doi.org/10.1002/joc.6860.

Kang, H., Sridhar, V., Mainuddin, M., Trung, L.D., 2021. Future rice farming threatened by drought in the lower Mekong Basin. Sci. Rep. 11 (1). https://doi.org/10.1038/s41598-021-88405-2.

Keenan, T.F., Hollinger, D.Y., Bohrer, G., Dragoni, D., Munger, J.W., Schmid, H.P., Richardson, A.D., 2013. Increase in forest water-use efficiency as atmospheric

carbon dioxide concentrations rise. Nature 499 (7458), 324–327. https://doi.org/10.1038/nature12291.
Krishnaswamy, J., John, R., Joseph, S., 2013. Consistent response of vegetation dynamics to recent climate change in tropical mountain regions. Glob. Chang. Biol. 20 (1), 203–215. https://doi.org/10.1111/gcb.12362.
Lao PDR, 2013. Second National Communication to the UNFCCC. Ministry of Natural Resources and Environment, Vientiane, Lao PDR. Retrieved from. https://unfccc.int/sites/default/files/resource/Laonc2.pdf.
Lao PDR, 2021. Climate Risk Country Profile. The World Bank Group and the Asian Development Bank. Retrieved from. https://www.adb.org/sites/default/files/publication/709846/climate-risk-country-profile-lao-pdr.pdf.
Lumyai, P., Palakit, K., Duangsathaporn, K., Wanthongchai, K., 2020. A 324-years temperature reconstruction from *Pinus latteri* Mason at highland in Chiang Mai Province, Thailand. Biodiversitas 21 (9). https://doi.org/10.13057/biodiv/d210903.
Maniphousay, V., 2021. Climate change adaptation in Lao PDR. In: Disaster Risk Reduction, pp. 77–102. https://doi.org/10.1007/978-981-16-6088-7_5.
Mann, M.E., Lees, J.M., 1996. Robust estimation of background noise and signal detection in climatic time series. Clim. Chang. 33 (3), 409–445. https://doi.org/10.1007/bf00142586.
McPhaden, M.J., Zebiak, S.E., Glantz, M.H., 2006. ENSO as an integrating concept in earth science. Science 314 (5806), 1740–1745. https://doi.org/10.1126/science.1132588.
Meko, D., Graybill, D.A., 1995. Tree-ring reconstruction of upper Gila Rwer discharge. J. Am. Water Resour. Assoc. 31 (4), 605–616. https://doi.org/10.1111/j.1752-1688.1995.tb03388.x.
Mekong River Commission. (2019). MRC State of Basin Report 2018 — Summary Version. https://www.mrcmekong.org/wp-content/uploads/2024/08/Summary-State-of-the-Basin-Report-2018.pdf.
Michaelsen, J., 1987. Cross-validation in statistical climate forecast models. J. Clim. Appl. Meteorol. 26 (11), 1589–1600. https://doi.org/10.1175/1520-0450(1987)026.
Miyan, M.A., 2015. Droughts in Asian least developed countries: Vulnerability and sustainability. Weather Clim. Extremes 7, 8–23. https://doi.org/10.1016/j.wace.2014.06.003.
Mukherjee, S., Mishra, A., Trenberth, K.E., 2018. Climate change and drought: a perspective on drought indices. Curr. Clim. Chang. Rep. 4 (2), 145–163. https://doi.org/10.1007/s40641-018-0098-x.
Naumthong, M., Palakit, K., Duangsathaporn, K., Prasomsin, P., Lumyai, P., 2021. Climate effects on the growth of *Pinus latteri* and *Pinus kesiya* at the Intakin Silvicultural Research Station, Chiang Mai Province, Thailand. Biodiversitas 22 (5). https://doi.org/10.13057/biodiv/d220508.
Nguyen, T.T.H., Li, M.H., Vu, T.M., Chen, P.Y., 2023. Multiple drought indices and their teleconnections with ENSO in various spatiotemporal scales over the Mekong River Basin. Sci. Total Environ. 854, 158589. https://doi.org/10.1016/j.scitotenv.2022.15858.
Panthi, S., Bräuning, A., Zhou, Z.K., Fan, Z.X., 2017. Tree rings reveal recent intensified spring drought in the central Himalaya, Nepal. Glob. Planet. Chang. 157, 26–34. https://doi.org/10.1016/j.gloplacha.2017.08.012.
Phan-Van, T., Nguyen-Ngoc-Bich, P., Ngo-Duc, T., Vu-Minh, T., Le, P.V.V., Trinh-Tuan, L., Nguyen-Thi, T., Pham-Thanh, H., Tran-Quang, D., 2022. Drought over Southeast Asia and its association with large-scale drivers. J. Clim. 35 (15), 4959–4978. https://doi.org/10.1175/jcli-d-21-0770.1.
Pumijumnong, N., 2013. Dendrochronology in Southeast Asia. Trees 27 (2), 343–358. https://doi.org/10.1007/s00468-012-0775-7.
Pumijumnong, N., Eckstein, D., 2010. Reconstruction of pre-monsoon weather conditions in northwestern Thailand from the tree-ring widths of *Pinus merkusii* and *Pinus kesiya*. Trees 25 (1), 125–132. https://doi.org/10.1007/s00468-010-0528-4.
Pumijumnong, N., Palakit, K., 2020. Effects of climate variability on the annual and intra-annual ring formation of *Pinus merkusii* growing in Central Thailand. Environ. Natural Resour. J. Warasan Singwaetlom Lae Sappayakon Tammachat 18 (3), 234–248. https://doi.org/10.32526/ennrj.18.3.2020.22.
Pumijumnong, N., Wanyaphet, T., 2006. Seasonal cambial activity and tree-ring formation of *Pinus merkusii* and *Pinus kesiya* in Northern Thailand in dependence on climate. For. Ecol. Manag. 226 (1–3), 279–289. https://doi.org/10.1016/j.foreco.2006.01.040.
Pumijumnong, N., Songtrirat, P., Buajan, S., Preechamart, S., Chareonwong, U., Muangsong, C., 2021. Climate control of cambial dynamics and tree-ring width in two tropical pines in Thailand. Agric. For. Meteorol. 303, 108394. https://doi.org/10.1016/j.agrformet.2021.108394.
Pumijumnong, N., Muangsong, C., Panthi, S., Buajan, S., Cai, B., Kulsuwan, P., Kongsombat, P., 2023. A 225-year pine (*Pinus latteri*) tree-ring record of pre-monsoon relative humidity variation in Nan province of northern Thailand and the linkage with large-scale ocean-atmospheric circulations. Glob. Planet. Chang. 230, 104277. https://doi.org/10.1016/j.gloplacha.2023.104277.
R Core Team, 2024. R: A Language and Environment for Statistical Computing. The R Foundation for Statistical Computing, Vienna. https://www.r-project.org/.
Rakthai, S., Fu, P.L., Fan, Z.X., Gaire, N., Pumijumnong, N., Eiadthong, W., Tangmitcharoen, S., 2020. Increased drought sensitivity results in a declining tree growth of *Pinus latteri* in Northeastern Thailand. Forests 11 (3), 361. https://doi.org/10.3390/f11030361.
Räsänen, T.A., Lindgren, V., Guillaume, J.H.A., Buckley, B.M., Kummu, M., 2016. On the spatial and temporal variability of ENSO precipitation and drought teleconnection in mainland Southeast Asia. Clim. Past 12 (9), 1889–1905. https://doi.org/10.5194/cp-12-1889-2016.
Rinn, F., 2003. TSAP-Win User Reference Manual. Rinntech, Heidelberg.
Ruiz-Barradas, A., Nigam, S., 2018. Hydroclimate variability and change over the Mekong River Basin: Modeling and predictability and policy implications. J. Hydrometeorol. 19 (5), 849–869. https://doi.org/10.1175/jhm-d-17-0195.1.
Sano, M., Buckley, B.M., Sweda, T., 2009. Tree-ring based hydroclimate reconstruction over northern Vietnam from *Fokienia hodginsii*: eighteenth century mega-drought and tropical Pacific influence. Clim. Dyn. 33 (2–3), 331–340. https://doi.org/10.1007/s00382-008-0454-y.
Sano, M., Xu, C., Nakatsuka, T., 2012. A 300-year Vietnam hydroclimate and ENSO variability record reconstructed from tree ringδ18O. J. Geophys. Res. 117 (D12). https://doi.org/10.1029/2012jd017749.
Sein, Z.M.M., Zhi, X., 2016. Interannual variability of summer monsoon rainfall over Myanmar. Arab. J. Geosci. 9 (6). https://doi.org/10.1007/s12517-016-2502-y.
Sharma, B., Fan, Z.X., Panthi, S., Gaire, N.P., Fu, P.L., Zaw, Z., 2022. Warming induced tree-growth decline of *Toona ciliata* in (sub-) tropical southwestern China. Dendrochronologia 73, 125954. https://doi.org/10.1016/j.dendro.2022.125954.
Shekhar, M., Sharma, A., Dimri, A., Tandon, S.K., 2022. Asian summer monsoon variability, global teleconnections, and dynamics during the last 1,000 years. Earth Sci. Rev. 230, 104041. https://doi.org/10.1016/j.earscirev.2022.104041.
Stephens, S.L., Agee, J.K., Fulé, P.Z., North, M.P., Romme, W.H., Swetnam, T.W., Turner, M.G., 2013. Managing forests and fire in changing climates. Science 342 (6154), 41–42. https://doi.org/10.1126/science.1240294.
Stibig, H.J., Achard, F., Carboni, S., Raši, R., Miettinen, J., 2014. Change in tropical forest cover of Southeast Asia from 1990 to 2010. Biogeosciences 11 (2), 247–258. https://doi.org/10.5194/bg-11-247-2014.
Thomas, P., 2019. Pinus Latteri from the Website: “Threatened Conifers of the World”. https://threatenedconifers.rbge.org.uk/conifers/pinus-latteri.
Trenberth, K., Overpeck, J., Solomon, S., 2004. Exploring drought and its implications for the future. Eos 85 (3), 27. https://doi.org/10.1029/2004eo030004.
Trenberth, K.E., Dai, A., Van Der Schrier, G., Jones, P.D., Barichivich, J., Briffa, K.R., Sheffield, J., 2014. Global warming and changes in drought. Nat. Clim. Chang. 4 (1), 17–22. https://doi.org/10.1038/nclimate2067.
Trouet, V., Van Oldenborgh, G.J., 2013. KNMI climate Explorer: a web-based research tool for high-resolution paleoclimatology. Tree-ring Res. 69 (1), 3–13. https://doi.org/10.3959/1536-1098-69.1.3.
Ummenhofer, C.C., D’Arrigo, R.D., Anchukaitis, K.J., Buckley, B.M., Cook, E.R., 2013. Links between Indo-Pacific climate variability and drought in the Monsoon Asia Drought Atlas. Clim. Dyn. 40 (5–6), 1319–1334. https://doi.org/10.1007/s00382-012-1458-1.
UNDRR, 2013. Country Assessment Report for Lao PDR. United Nations Office for Disaster Risk Reduction (UNDRR). Retrieved from. https://www.unisdr.org/files/33988_countryassessmentreportlaopdr%5B1%5D.pdf.
Vicente-Serrano, S.M., Beguería, S., López-Moreno, J.I., 2010. A multiscalar drought index sensitive to global warming: the standardized Precipitation Evapotranspiration Index. J. Clim. 23 (7), 1696–1718. https://doi.org/10.1175/2009jcli2909.1.
Vlam, M., Baker, P.J., Bunyavejchewin, S., Zuidema, P.A., 2014. Temperature and rainfall strongly drive temporal growth variation in Asian tropical forest trees. Oecologia 174 (4), 1449–1461. https://doi.org/10.1007/s00442-013-2846-x.
Wang, B., Wu, R., Fu, X., 2000. Pacific–East Asian teleconnection: How does ENSO affect East Asian climate? J. Clim. 13 (9), 1517–1536. https://doi.org/10.1175/1520-0442(2000)013<1517:PEATHD>2.0.CO;2.
Wang, Y.V., Larsen, T., Lauterbach, S., Andersen, N., Blanz, T., Krebs-Kanzow, U., Gierz, P., Schneider, R.R., 2022. Higher sea surface temperature in the Indian Ocean during the last Interglacial weakened the south Asian monsoon. Proc. Natl. Acad. Sci. USA 119 (10). https://doi.org/10.1073/pnas.2107720119.
Weldeab, S., Rühlemann, C., Ding, Q., Khon, V., Schneider, B., Gray, W., 2022. Impact of Indian Ocean surface temperature gradient reversals on the Indian Summer Monsoon. Earth Planet. Sci. Lett. 578, 117327. https://doi.org/10.1016/j.epsl.2021.117327.
Wigley, T.M.L., Briffa, K.R., Jones, P.D., 1984. On the average value of correlated time series, with applications in Dendroclimatology and hydrometeorology. J. Clim. Appl. Meteorol. 23 (2), 201–213. https://doi.org/10.1175/1520-0450(1984)023.
Wilcove, D.S., Giam, X., Edwards, D.P., Fisher, B., Koh, L.P., 2013. Navjot’s nightmare revisited: logging, agriculture, and biodiversity in Southeast Asia. Trends Ecol. Evol. 28 (9), 531–540. https://doi.org/10.1016/j.tree.2013.04.005.
Xu, C., Sano, M., Nakatsuka, T., 2011. Tree ring cellulose δ^{18}O of *Fokienia hodginsiiin* northern Laos: a promising proxy to reconstruct ENSO? J. Geophys. Res. 116 (D24). https://doi.org/10.1029/2011jd016694.
Xu, C., Pumijumnong, N., Nakatsuka, T., Sano, M., Li, Z., 2015. A tree-ring cellulose δ^{18}O-based July–October precipitation reconstruction since AD 1828, Northwest Thailand. J. Hydrol. 529, 433–441. https://doi.org/10.1016/j.jhydrol.2015.02.037.
Xu, T.L., Yang, R.Q., Zaw, Z., Fu, P.L., Panthi, S., Bräuning, A., Fan, Z.X., 2024. Growth-climate relationships of four tree species in the subtropical evergreen broad-leaved forests in Southwest China. Dendrochronologia 85, 126186. https://doi.org/10.1016/j.dendro.2024.126186.
Yang, R.Q., Fu, P.L., Fan, Z.X., Panthi, S., Gao, J., Niu, Y., Li, Z.S., Bräuning, A., 2022. Growth-climate sensitivity of two pine species shows species-specific changes along temperature and moisture gradients in Southwest China. Agric. For. Meteorol. 318, 108907. https://doi.org/10.1016/j.agrformet.2022.108907.
Yao, J., Tuoliewubieke, D., Chen, J., Huo, W., Hu, W., 2019. Identification of drought events and correlations with large-scale ocean-atmospheric patterns of variability: a case study in Xinjiang, China. Atmosphere 10 (2), 94. https://doi.org/10.3390/atmos10020094.
Yin, H., Wu, Z., Fowler, H.J., Blenkinsop, S., He, H., Li, Y., 2022. The combined impacts of ENSO and IOD on global seasonal droughts. Atmosphere 13 (10), 1673. https://doi.org/10.3390/atmos13101673.

Yin, Y.L., Zaw, Z., Peng, X.H., Zhang, H., Fu, P.L., Wang, W.L., Bräuning, A., Fan, Z.X., 2023. Tree rings in *Tsuga dumosa* reveal increasing drought variability in subtropical Southwest China over the past two centuries. Palaeogeogr. Palaeoclimatol. Palaeoecol. 628, 111757. https://doi.org/10.1016/j.palaeo.2023.111757.

Zaw, Z., Fan, Z., Bräuning, A., Xu, C., Liu, W., Gaire, N.P., Panthi, S., Than, K.Z., 2020. Drought reconstruction over the past two centuries in southern Myanmar using teak tree-rings: Linkages to the Pacific and Indian Oceans. Geophys. Res. Lett. 47 (10). https://doi.org/10.1029/2020gl087627.

Zaw, Z., Fan, Z.X., Bräuning, A., Liu, W., Gaire, N.P., Than, K.Z., Panthi, S., 2021. Monsoon precipitation variations in Myanmar since AD 1770: linkage to tropical ocean-atmospheric circulations. Clim. Dyn. 56 (9–10), 3337–3352. https://doi.org/10.1007/s00382-021-05645-8.

Zhang, L., Song, W., Song, W., 2020. Assessment of agricultural drought risk in the Lancang-Mekong Region, South East Asia. Int. J. Environ. Res. Public Health 17 (17), 6153. https://doi.org/10.3390/ijerph17176153.

Zhu, M., Stott, L., Buckley, B., Yoshimura, K., Ra, K., 2012. Indo-Pacific warm Pool convection and ENSO since 1867 derived from Cambodian pine tree cellulose oxygen isotopes. J. Geophys. Res. 117 (D11). https://doi.org/10.1029/2011jd017198.

Zuidema, P.A., Babst, F., Groenendijk, P., Trouet, V., Abiyu, A., Acuña-Soto, R., et al., 2022. Tropical tree growth driven by dry-season climate variability. Nat. Geosci. 15 (4), 269–276. https://doi.org/10.1038/s41561-022-00911-8.